PREDICTABILITY OF THE STATISTICAL PROPERTIES OF LOW-FREQUENCY VARIABILITY: INFLUENCE OF CHAOTIC DYNAMICS AND BOUNDARY FORCING

Franco Molteni[1] *and* Susanna Corti[2]

[1] *CINECA - Centro di Calcolo Interuniversitario dell'Italia Nord-Orientale*
Casalecchio di Reno, Bologna, Italy
[2] *Atmospheric Dynamics Group, Department of Physics*
University of Bologna, Italy

SUMMARY

The predictability of statistical properties of low-frequency variability is investigated by studying the dynamical origin of both the 'signal' and the 'noise', which arise respectively from the non-linear response to variations in atmospheric forcing and from chaotic fluctuations in the energy partition between different variability patterns. Results from long integrations of a realistic quasi-geostrophic (QG) model are analysed, and interpreted on the basis of the behaviour of simple non-linear dynamical systems. It is shown that chaotic energy fluctuations not only modify the variance explained by different variability patterns, but may either obscure or enhance the multimodality in the distribution of model states in periods as long as several decades. On the other hand, it is argued that significant variations in atmospheric statistics may be induced by anomalies in the atmospheric forcing originated from the lower boundary. QG simulations show that a strengthening of the planetary-wave forcing due to the asymmetry in the divergent circulation between the western and eastern Pacific increases low-frequency variability in the extratropical Pacific, and may turn the distribution of model states from unimodal to bimodal. Anomalies in low-frequency variance related to changes in atmospheric forcing seem to be larger than those originated by internal dynamics, at least in certain periods and regions, suggesting a potential predictability of these statistics by coupled ocean-atmosphere models.

1. INTRODUCTION.

The analysis of the amplitude and spatial distribution of atmospheric variability is a fundamental part of the study of the Earth's climate. Therefore, a detailed comparison between observed and simulated variability is essential for a proper validation of general circulation models (GCMs). While a decade ago studies on the 'systematic' error of GCMs were mainly focussed on errors in the time-mean, more recently errors in modelled variability have been thoroughly investigated and documented (e.g. Ferranti et al. 1994b; Chen and Van den Dool 1995).

In numerical weather prediction (NWP), the importance of a correct simulation of atmospheric variability has long been recognized. However, as the time-range of skilful predictions has been extended from a few days to one week or longer, the emphasis has been shifted from high-frequency midlatitude transients (i.e. baroclinic waves) to low-frequency variability modes in both extratropical and tropical regions. It was found

that a large proportion of the 'systematic' error of medium- and extended-range forecasts is related to the inability of models to simulate correctly the frequency of occurrence of large-scale flow-regimes (e.g. Tibaldi and Molteni 1990; Tracton et al. 1989; Miyakoda and Sirutis 1990). With the recent progress in ensemble predictions, both for operational medium-range forecasts (Tracton and Kalnay 1993; Molteni et al. 1996) and for experimental seasonal-scale prediction (recently reviewed by Palmer and Anderson 1994), a proper representation of atmospheric low-frequency variability has become indispensable for a correct estimate of the probabilistic distribution of atmospheric states. Indeed, estimates of atmospheric predictability (as well as of forecast skill) obtained by numerical integrations crucially depend on the level of internal model variability, as shown by Simmons et al. (1995) even in the context of 'deterministic' NWP.

Several aspects of a model formulation may affect the amount of variability generated by its internal dynamics. In forced, dissipative non-linear systems, energy is injected into the system by forcing, and is removed by dissipation. In general, an increase in the intensity of the energy source leads to increased variability, while stronger dissipative processes tend to reduce it. As far as the forcing terms are concerned, however, their spatial structure is crucial in determining their 'efficiency' as a source of variability. This dependence of variability on the amplitude and structure of the energy source is often obscured in studies which explain atmospheric variability in terms of linear instabilities of the time-mean flow, because a time-independent forcing disappears from the linearised equations, and its influence is only implicitly felt through the basic state. Andrews (1984) pointed out that different assumptions on the nature of the forcing which maintains a given basic state may lead to different conclusions on the instability of the flow.

Although for the climate system as a whole the only 'external' energy source is solar radiation, the forcing felt by the atmosphere alone is strongly modulated by the boundary conditions at the Earth's surface. As long as these boundary conditions (especially the sea surface temperature, SST) can be predicted on the seasonal to interannual time scale, the possibility arises of a prediction not only of the time-mean but also of some statistical properties of the atmospheric variability. Up to now, studies on seasonal predictability have concentrated on predictions of the seasonal-mean flow. However, information on the amount of low-frequency variability may be of great importance to estimate the probability of extreme anomalies within a season.

Understanding how variability depends on the atmospheric forcing is not only relevant for extended-range predictions. Deficiencies in the parametrization of physical processes in GCMs result in modelled energy sources which may differ from those of the real atmosphere in intensity, spatial distribution and flow-dependence. The search for the origin of systematic errors which affect medium-range forecasts may therefore benefit from a deeper knowledge of the relationship between variability and forcing. Ferranti et

al. (1994a) showed that correcting a systematic error of the ECMWF model in tropical rainfall distribution by a time-independent anomalous forcing (namely, a warm SST anomaly in the Indonesian region) dramatically improved the model's ability to simulate blocking frequency in the northern extratropics.

The main difficulty in diagnosing (and eventually predicting) the effects of forcing on atmospheric variability is that sampling problems, already affecting the estimate of the time-mean state, become even more serious for second-order moments. Differences in intraseasonal variability between different years may well arise from the chaotic nature of the atmospheric dynamics rather than from differences in external forcing. It is therefore important to develop techniques to quantify this 'dynamical noise', and distinguish it from the 'signal' coming from forcing variations. As shown later, standard statistical tests based on red-noise signals may not be adequate for this purpose when applied to chaotic systems with a very large number of degrees of freedom.

This study addresses the problems discussed above by analysing results from long integrations of a 3-level quasi-geostrophic model, which is able to generate realistic low-frequency variability in the northern extratropics (see Marshall and Molteni 1993; Liu and Opsteegh 1995; Molteni 1996). The paper is organized as follows. In Sect. 2 the amount and distribution of observed intraseasonal variability in different years is discussed, with reference to the possible links with SST anomalies. In Sect. 3, two dynamical approaches to the estimate of low-frequency variability are presented, based respectively on linear and non-linear theory. Sect. 4 is concerned with the 'dynamical noise', that is with the dynamical processes that may cause fluctuations in the internal variability of the model on the interannual (or even interdecadal) time scale. Sect. 5 is instead concerned with the 'signal' coming from boundary forcing: it will be shown that interannual differences in extratropical variability may be modelled (and are therefore potentially predictable) as a response to anomalies in tropical heat sources. Conclusions will be drawn in Sect. 6.

2. INTERANNUAL CHANGES IN LOW-FREQUENCY VARIABILITY: OBSERVATIONS.

In this section, observational evidence on the interannual changes in the amount and distribution of low-frequency variability will be briefly presented, and a possible relationship with features of the time-mean flow and anomalies in atmospheric boundary conditions will be discussed. As in the rest of the paper, attention will be focussed on the northern winter, and particularly on the January and February months, which represent a fairly homogeneous period for the statistics of the atmospheric circulation. As pointed out by Livezey (1994, personal communication), it is also a more homogeneous period than the 'traditional' December-to-February winter as far as the response of the northern extratropical atmosphere to anomalous forcing of tropical origin is concerned.

In a study of high-frequency, baroclinically unstable disturbances, it would be natural to look for a relationship between their amplitude and the strength of the zonal-mean flow. In the case of intraseasonal low-frequency variability, theoretical and modelling evidence rather suggests a relationship with the amplitude and phase of the planetary waves, which has been often interpreted on the basis of the barotropic instability of a zonally asymmetric basic state (e.g Simmons et al. 1983; Branstator 1985; Palmer 1988). To investigate such a relationship, Figs. 1 and 2 show in the upper panels the time-mean, zonally-asymmetric (eddy) component of 500 hPa height, averaged over January and February (JF hereafter) of different years, while in the lower panels the standard deviation of 5-day-mean height anomalies in the same periods is plotted as a measure of low-frequency variability.

Figure 1 compares two winter periods characterised by almost opposite anomalies in both the extratropical mean flow and sea-surface temperature (SST) in the tropical Pacific, namely JF 1987 (warm ENSO phase) and JF 1989 (cold ENSO phase; e.g. Brankovic et al. 1994). The well-documented association between large anomalies in tropical Pacific SST and the phase of the Pacific-North American (PNA) teleconnection pattern (e.g Horel and Wallace 1981) is reflected in the different location of the quasi-stationary ridge in the PNA sector: centred over the Rocky Mountains in JF 1987 (positive PNA anomaly), over the north-eastern Pacific in JF 1989 (negative PNA anomaly). In JF 1989 the ridge has a slightly larger amplitude, while the trough associated with the Pacific storm track is confined to the western portion of the ocean. The amount and distribution of low-frequency variability in the Pacific-North American region is quite different in the two winters. In JF 1987, the Pacific maximum is localised in the eastern part of the ocean, with a peak of about 160 m; in JF 1989, the maximum exceeds 240 m and is shifted over Alaska, as a consequence of intense blocking episodes.

Before commenting on the situation in the Euro-Atlantic sector, let us analyse the mean eddies and variability fields in the Pacific during two further winter periods, JF 1991 and JF 1992; these are shown in Fig. 2. As 1987, 1992 was an "El Niño year" with warm SST anomalies in the eastern equatorial Pacific (see also Sect. 5b). In the extratropical Pacific, similarities between JF 1987 and 1992 are evident in both the mean eddies (the quasi-stationary ridge is not very strong, and shifted over the continent) and the low-frequency standard deviation (much below average in 1992, with a maximum just exceeding 140 m). The tendency for below-average low-frequency variability during El Niño winters is confirmed by the analysis of JF 1983 (not shown). JF 1991, on the other hand, is a winter period of weak anomalies in tropical SST, but of considerable intraseasonal variability in the extratropics. This is shown by the large standard-deviation in the eastern Pacific (see panel 2b) which exceeds 200 m over Alaska; as in JF 1989, the northern shift of the low-frequency variability maximum is associated with large blocking frequency in the region. Unlike JF 1989, however, the PNA pattern did not have a preferred phase, so that the eastern Pacific ridge had an 'intermediate' position cented just over the west coast of North America. The ridge was

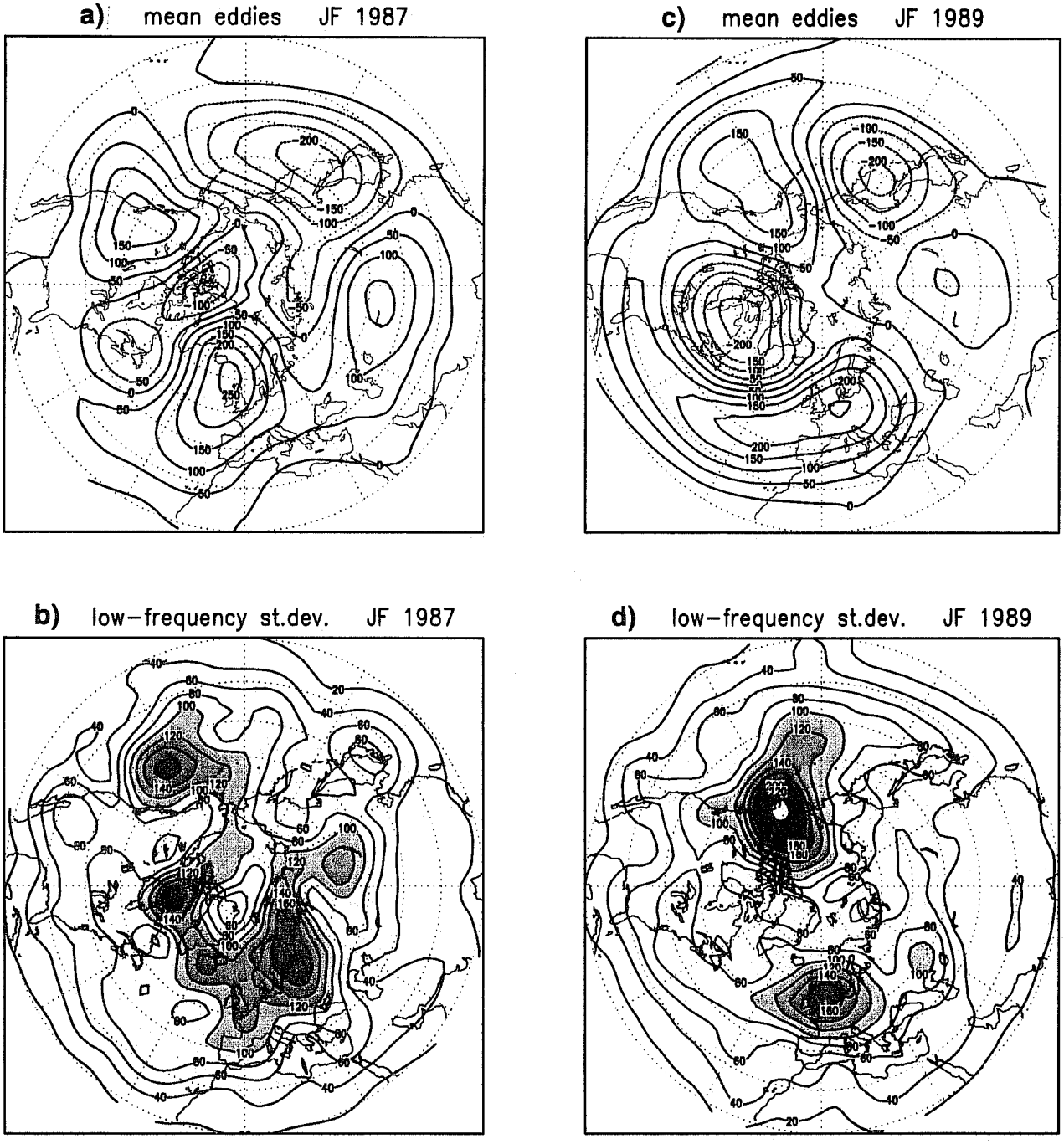

Fig. 1 a) Eddy component of the 500 hPa height field, averaged over January-February (JF) 1987; b) standard deviation of 5-day mean anomalies of 500 hPa height in JF 1987; c) and d): as in a) and b), but for JF 1989.

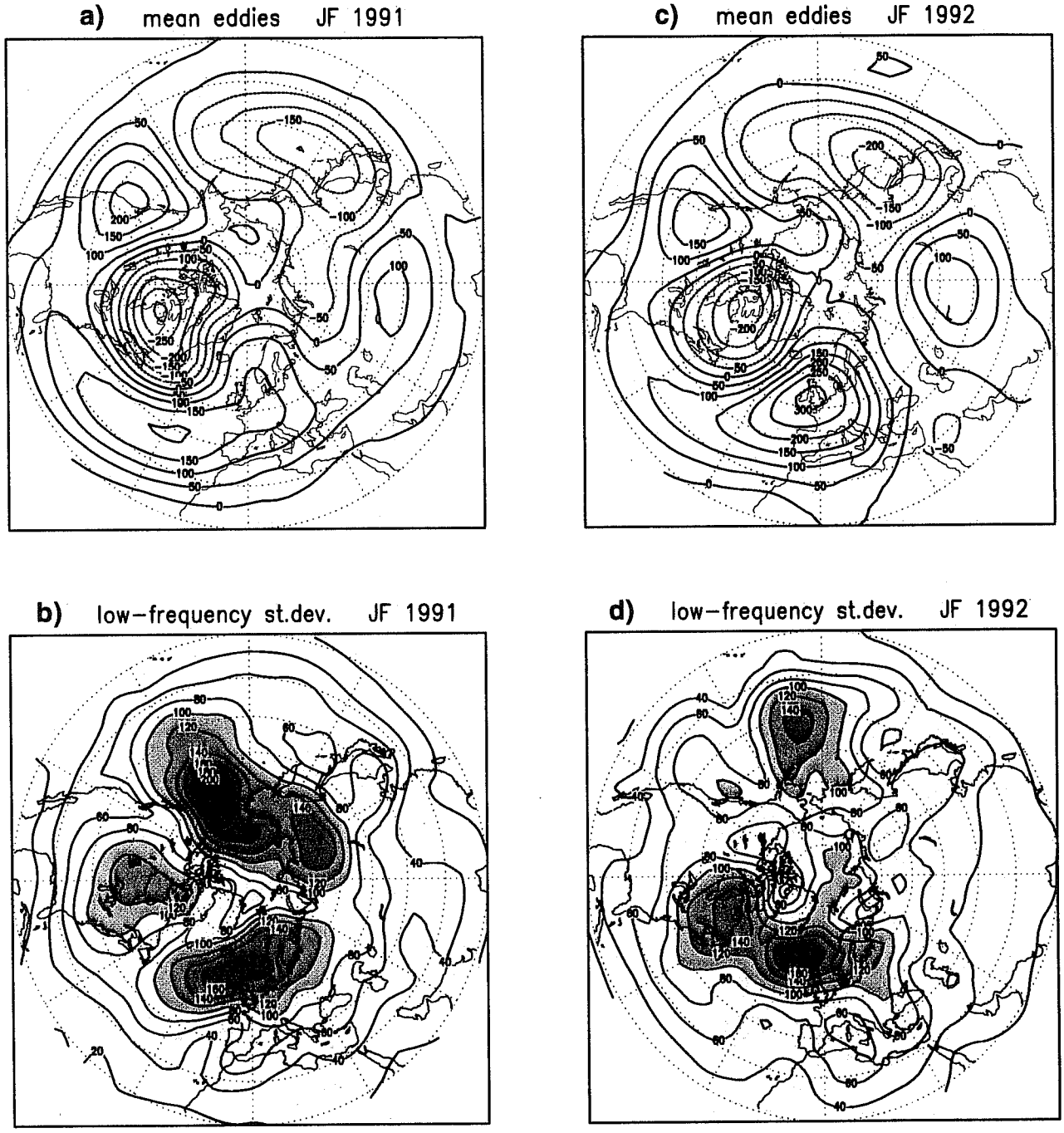

Fig. 2 a) Eddy component of the 500 hPa height field, averaged over January-February (JF) 1991. b) Standard deviation of 5-day mean anomalies of 500 hPa height in JF 1991; c) and d): as in a) and b), but for JF 1992.

anomalously strong in JF 1991, reflecting frequent episodes of planetary-wave amplification.

If, in the Pacific region, even a simple qualitative analyis seems to indicate a relationship between intraseasonal variability and properties of the quasi-stationary wave pattern (see also Palmer 1988), in the Euro-Atlantic sector the situation is more complex. One cannot see a simple relationship, for example, between amplitude of the time-mean eddies and amount of low-frequency variability. In JF 1991, the time-mean planetary waves over north-western Europe were weaker than in JF 1992, and still low-frequency standard deviation in the region was larger in the former period. Interannual variations in the maximum standard deviation appear to be smaller than in the Pacific region, but are at least comparable as far as the location of the maximum is concerned. The analysis of a much larger data sample is certainly needed to confirm these statements and reveal any significant relationship, which however is beyond the scope of this paper. Rather than going into a deeper observational analysis, we will investigate the dynamical aspects of the problem, using theoretical and numerical models of different complexity.

3. THEORETICAL ESTIMATES OF LOW-FREQUENCY VARIANCE.

In this section, simple theoretical arguments will be presented to find a dynamical relationship between atmospheric forcing and low-frequency variability. Let X be the state vector of a non-linear dynamical system, which will be assumed as a model of the atmosphere. The time evolution of X is given by:

$$\dot{X} = A(X,X) + B(X) + F_d \tag{1}$$

where A is a non-linear operator representing advective processes, B represents linear tendencies (including dissipative terms) and F_d is a forcing due to diabatic processes.

Following observational evidence (e.g. Dole 1983), let us assume that low-frequency variability is mainly due to the alternation of persistent large-scale flow patterns, separated by relatively fast transition periods. Such quasi-stationary states $\tilde{X}$ can be thought of as the solutions of the equation:

$$A(\tilde{X},\tilde{X}) + B(\tilde{X}) + \tilde{F}_d + \tilde{F}_{hf} = 0 \tag{2}$$

where $\tilde{F}_{hf}$ is the 'forcing' of the large-scale flow by high-frequency transients, averaged over the typical

lifetime τ of persistent anomalies (of the order of 10 days). If the operator $\{\ \}_\tau$ represents the time-average and X' indicates the high-frequency component of the state vector, then $\tilde{F}_d = \{F_d\}_\tau$ and $\tilde{F}_{hf} = \{A(X',X')\}_\tau$.

At this point, one can follow either a linear or a non-linear approach to the estimate of low-frequency variance. Starting with linear theory, let us define a 'season' as a time interval over which the diabatic forcing is approximately constant, and let us decompose $\tilde{X}$ into the sum of a seasonal mean $\bar{X}$ and a low-frequency anomaly X_a. If one assumes that for any X_a the non-linear term $A(X_a,X_a)$ can be neglected, then $\bar{X}$ and X_a satisfy respectively:

$$A(\bar{X},\bar{X}) + B(\bar{X}) + \bar{F}_d + \bar{F}_{hf} = 0 \tag{3a}$$

$$L X_a + F_a = 0 \tag{3b}$$

where in (3a) the diabatic and high-frequency forcings are averaged over the whole season, while in (3b) the linearised time-derivative operator L and the forcing anomaly F_a are given by :

$$L X_a = A(\bar{X},X_a) + A(X_a,\bar{X}) + B(X_a) \tag{4a}$$

$$F_a = \tilde{F}_d - \bar{F}_d + \tilde{F}_{hf} - \bar{F}_{hf} \tag{4b}$$

If n is the number of degrees of freedom of the dynamical system represented by Eq. 1, then X_a and F_a can be represented as vectors in an n-dimensional phase space, and L as a $n \times n$ matrix.

The information about the amplitude and spatial patterns of low-frequency variability is conveyed by the covariance matrix C_X of the anomalies X_a. In particular, the eigenvectors of C_X (usually referred to as empirical orthogonal functions, or EOFs) define an orthonormal base in phase space such that the subspace spanned by the m EOFs with the largest eigenvalues account for the largest possible proportion of variance among all the possible subspaces of dimension m. In order to relate the flow-anomaly covariance matrix C_X with the forcing-anomaly covariance matrix C_F, let us first write them respectively as:

$$C_X = \overline{X_a X_a^t} \tag{5a}$$

$$C_F = \overline{F_a F_a^t} \tag{5b}$$

where the superscript t denotes the transpose in the n-dimensional phase space and the overbar again indicates the average over the whole seasonal sample. Then, from Eq. 3b one obtains:

$$C_X = L^{-1}\, \overline{F_a F_a^t}\, (L^{-1})^t = L^{-1}\, C_f\, (L^{-1})^t \,. \tag{6}$$

If, as far as intra-seasonal variability is concerned, the forcing anomalies F_a are assumed to possess a white-noise structure, then $C_F = w I$ (where w is the white-noise variance and I is the identity matrix), and Eq. 6 becomes:

$$C_X = w (L^t L)^{-1} \,. \tag{7}$$

It follows that the leading EOFs, i.e. the eigenvectors of C_X with the *largest* eigenvalues, are equal to the eigenvectors of $L^t L$ with the *smallest* eigenvalues. Since L^t corresponds to the adjoint of the linearised time-derivative, it can be easily shown that the eigenvalues of $L^t L$ represent the squared norm of the time-derivative of the associated eigenvectors. Equation 7 implies that the EOF variances are inversely proportional to these eigenvalues. Therefore, the leading EOFs correspond here to linearly quasi-resonant anomalies, which can be maintained by forcing anomalies of small amplitude.

The relationship outlined above was derived by Navarra (1993), who pointed out that the eigenvectors of $L^t L$ are equivalent to the right singular vectors of L, while the forcing anomalies which balance such vectors are given by the associated left singular vectors. However, the concept that low-frequency EOFs correspond to quasi-resonant patterns emerging as a linear response to white-noise forcing anomalies can be traced back to earlier studies. Branstator (1990) compared streamfunction EOFs computed from the result of a 1200-day perpetual winter integration of NCAR's Climate Community Model with the EOFs of a set of 1000 streamfunction anomalies obtained as linear responses to randomly-distributed diabatic forcings. For two such EOFs, describing large-scale wave patterns in the Pacific (see Fig. 3), he found a good correspondence between the non-linear and the linear model, although the ranking of the EOFs was not the same. Similar

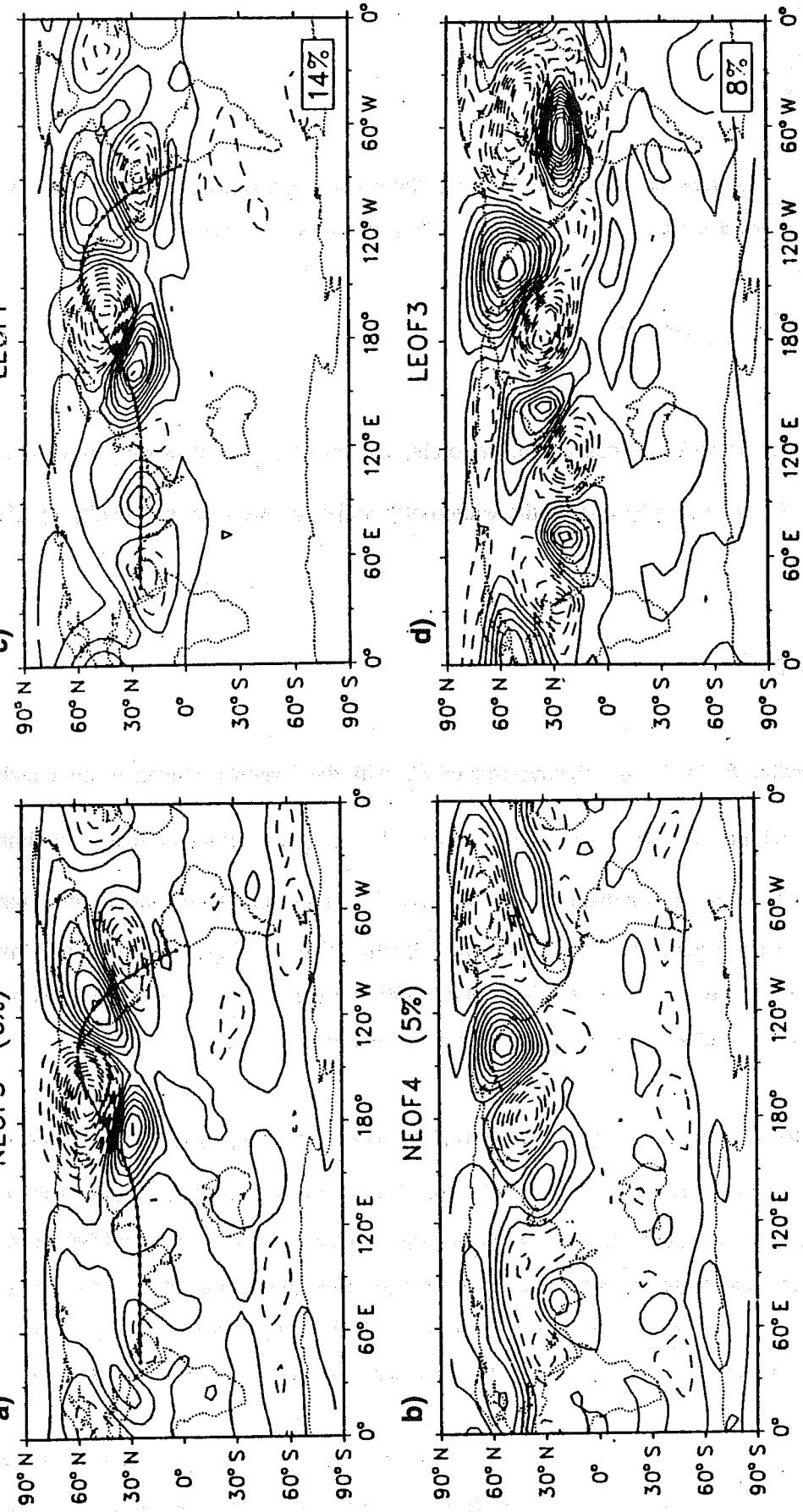

Fig. 3 a) and b): EOFs 3 and 4 of 300 hPa streamfunction from a 1200-day perpetual-winter integration of the NCAR CCM; c) and d): EOFs 1 and 2 of the linear response to white-noise temperature forcing (from Branstator 1990).

results were obtained using white-noise vorticity (instead of temperature) forcings for the linear model.

In this theory, if the white noise variance w is taken as a constant, the intensity and preferred spatial patterns of low-frequency variability are entirely determined by the dynamical properties of the linear operator L, in which the seasonally-averaged forcing $\bar{F}_d + \bar{F}_{hf}$ does not appear explicitely. However, the structure of the operator depends on the seasonal mean flow $\bar{X}$ used as a basic state, which in turn depends on the mean forcing. Branstator (1990) pointed out that quasi-resonant patterns such as those in Fig. 3c-d are able to extract energy from the basic state to compensate the energy loss due to dissipation, and noted that the existence of stationary waves in the basic states was crucial to the efficiency of this energy conversion process.

A similar result was obtained by Marshall and Molteni (1993), who computed eigenvectors of $L^t L$ using a three-level quasi-geostrophic (QG) model and basic states derived from both observed and modelled time-mean fields. They found that progressively reducing the amplitude of planetary-waves in the observed climatological basic state led to an increase of the smallest eigenvalues of $L^t L$. From the theory above, this implies that (for a given white-noise forcing) a stronger wave amplitude leads to a larger variance associated with the leading EOFs. Marshall and Molteni used the term 'neutral vectors' to define the eigenvectors of $L^t L$ with very small linear tendency, as a generalization of the term 'neutral modes' used for the normal modes of L with near-zero growth rate.

The linear theory outlined here seems able to justify the positive correlation between wave amplitude in the time-mean flow and intensity of low-frequency variance discussed in the previous section. However, if one wants to relate the changes in low-frequency variability to changes in atmospheric forcing, one has first to solve the non-linear steady-state problem for the seasonal-mean flow expressed by Eq. 3a. Attempts to use linear theory to estimate the seasonal-mean flow anomaly as the linear response to a seasonal-mean forcing anomaly had a moderate success only for strongly anomalous forcings (typically, in the case of the 1982/83 El Niño), as proved by the work of Navarra and Miyakoda (1988).

On the other hand, non-linear dynamics may be used to investigate changes in both mean state and intraseasonal variability without the need to split the problem into two parts. To do so, one may assume that low-frequency variability arises from the alternation of multiple flow-regimes, corresponding to multiple non-linear solution of Eq. 2. In this hypothesis, the leading patterns of low-frequency variability correspond to the axes connecting the different solutions in phase space, and the total amount of variability is

(approximately) proportional to the phase-space distance between these solutions.

Lorenz's (1963) 3-variable convection model provides a clear example of how the problem can be approached. It is instructive to rewrite Lorenz's model in such a way to define a suitable quadratic invariant, which may be conserved, generated or dissipated by various terms in the equations. As suggested by Lorenz himself, this can be accomplished by the change of variable:

$$W = r + \sigma - Z \; ; \tag{8}$$

for brevity, we refer to Lorenz (1963) for the meaning of the variables and parameters of this system. The prognostic equations of the model become:

$$\dot{X} = \sigma Y - \sigma X \tag{9a}$$

$$\dot{Y} = XW - \sigma X - Y \tag{9b}$$

$$\dot{W} = -XY - bW + b(r+\sigma) \tag{9c}$$

where the terms in the first two columns conserve the quantity $(X^2+Y^2+Z^2)$, those in the third column dissipate it, while the last term in Eq. 9c represents the 'energy source' for the motion. It is well known that the system possesses either one or three steady states according to whether the parameter r is less or greater than one, and that a strange attractor is obtained for r greater than a critical threshold, when all three steady states are unstable. The two 'wings' of the attractor originate from oscillations around two weakly-unstable steady states having the same W coordinate and opposite values of X and Y, given by:

$$X_s = Y_s = \pm\sqrt{b(r-1)} \; , \qquad W_s = \sigma + 1 \; . \tag{10}$$

As discussed in many papers (see Fig. 4a from Mo and Ghil 1987), the axis linking these two steady states is the leading EOF of the system. A suitable time filter can reveal a clear bimodality in the projection of the state vector along this axis, corresponding to the existence of two regimes associated with opposite senses of rotation of the convective cells (Marshall and Molteni 1993; see Fig. 4b). It can be verified that the variance along this axis is proportional to the squared distance between the two weakly-unstable steady states. According to Eq. 10, such squared distance is in turn linearly related to the time-independent forcing term on the right-hand-side of Eq. 9c.

To what extent this approach can be applied to the real atmosphere is a subject of debate. One should point out that in the Lorenz model the 'centroids' of the regimes are very close to the steady states of the

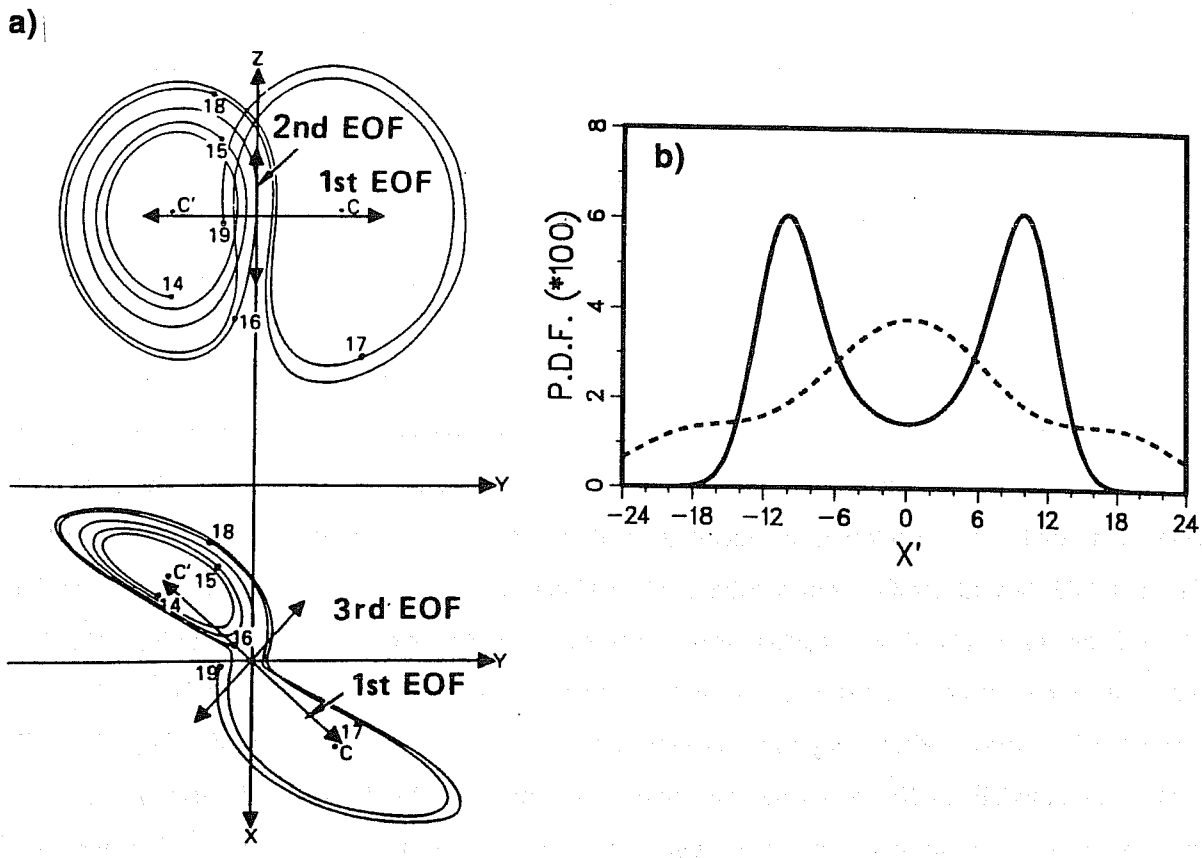

Fig. 4 a) EOFs of Lorenz's (1963) convection model (from Mo and Ghil 1987); b) Probability density function (PDF) for the projection of model states onto the first EOF: dashed line for unfiltered data, solid line for time-filtered data (from Marshall and Molteni 1993).

instantaneous flow; this means that the effects of 'high-frequency' transients (which appear in Eq. 2) are relatively unimportant as far as the regime position in phase space is concerned. This is certainly not the case for the real atmosphere, or for any realistic model of it. Indeed, even from the pioneering study of Reinhold and Pierrehumbert (1982) it emerged that baroclinically unstable transients were able to shift considerably the position of regimes centroids in phase space with respect to the steady states of the instantaneous flow. Vautard and Legras (1988) have shown that multiple flow regimes, defined as solutions of Eq. 2, may exist even in the presence of one single steady state for the instantaneous flow (i.e., of one single steady state of Eq. 1).

Is there any objective way to verify whether the linear or the non-linear methodology better explains the amount and stucture of intraseasonal variability? One may be tempted to interpret a similarity between actual EOFs and neutral vectors as a confirmation of the validity of linear thory. However, Marshall and Molteni (1993; MM93 herefter) showed that if a non-linear system possesses two regimes which are located in a fairly symmetrical position in phase space with respect to the time-mean state (as in the Lorenz model above), then the difference field between the two regimes is close to be a neutral vector for the linearised equations of motions. Indeed, they found statistical evidence of multiple regimes in the projections of both observed and modelled fields along neutral vectors. As confirmed by the study of Ferranti et al. (1994a), neutral vectors are a powerful linear tool to analyse low-frequency variability, but their similarity with actual anomalies is not a proof that non-linearity can be neglected.

4. VARIATIONS IN ATMOSPHERIC STATISTICS INDUCED BY INTERNAL DYNAMICS.

A detailed modelling study of the non-linear relationship between low-frequency variability and atmospheric forcing should be based on an analysis of the stationary and quasi-stationary solutions of the dynamical model employed. Until recently, such an analysis was only possible for models of a few to about a hundred degrees of freedom, which only allowed a qualitative comparison between observed and simulated variability patterns (e.g. Legras and Ghil 1985; Mukougawa 1988). For models of greater complexity and for the real atmosphere, the search for multiple regimes has often relied on the detection of multimodality in the probability density function (PDF) of parameters representative of the large-scale motion, like the amplitude of planetary waves (Hansen and Sutera 1986, 1990; Molteni et al. 1988) or the projections on selected EOFs (Molteni et al. 1990; Kimoto and Ghil 1993) and neutral vectors (MM93). Detection of multimodality with large statistical confidence is however very difficult in data samples as long as the whole record of post-war upper-air-field analyses (see the debate on the bimodality of the wave-amplitude index: Nitsche et al. 1994, Hansen and Sutera 1995). In addition, cases have been documented of multimodal signals that appeared in parts of long simulations with numerical models, but vanished in subsequent integrations, despite passing

statistical significance tests (Hansen, Malguzzi, personal communications). In this section, we will advocate that this phenomenon is related to dynamically-induced fluctations in the distribution of variance between different low-frequency variability patterns, which can be observed in many realistic models of the atmospheric flow.

a) The double Lorenz model.

To illustrate our ideas in a simple context, let us first consider a 5-variable dynamical system obtained by coupling two Lorenz models (as given by Eq. 9) in such a way that they share the W variable. The prognostic equations for this system read:

$$\dot{X}_1 = (\sigma + \alpha Y_2) Y_1 - \sigma X_1 \tag{11a}$$

$$\dot{Y}_1 = X_1 W - (\sigma + \alpha Y_2) X_1 - Y_1 \tag{11b}$$

$$\dot{X}_2 = (\sigma + \alpha Y_1) Y_2 - \sigma X_2 \tag{11c}$$

$$\dot{Y}_2 = X_2 W - (\sigma + \alpha Y_1) X_2 - Y_2 \tag{11d}$$

$$\dot{W} = -X_1 Y_1 - X_2 Y_2 - bW + b(r + \sigma) \tag{11e}$$

It can be immediately verified that, by setting either (X_1, Y_1) or (X_2, Y_2) to zero, the system is reduced to the 'single' Lorenz model in Eq. 9. Therefore, the 'double' system has five steady states, one in which only W is different from zero, two in which (X_1, Y_1, W) are given by Eq. 10 while (X_2, Y_2) are equal to zero, and two in which (X_2, Y_2, W) are given by Eq. 10 while (X_1, Y_1) vanish; regimes are associated with the latter four steady states. The role of the terms proportional to α in Eq. 11 is to prevent the system to behave as a 3-dimensional system, and to modify the stability properties of the steady states in such a way as to allow transitions from the regimes of subsystem (X_1, Y_1, W) to those of subsystem (X_2, Y_2, W).

In this model, regime transitions occur on a time scale of 1-2 time units; in the real atmosphere, the transition time-scale is 10-20 days. One can therefore assume that one time unit of the Lorenz model corresponds to 10 days in the atmosphere. The double Lorenz model has been integrated for 7200 time units (after a suitable spin-up time), setting $\alpha = 0.05$ and all the other parameters as in Lorenz (1963). Statistics of model variables have been computed for the full sample and for 20 subsamples of 360 time units (each one equivalent to the observed upper-air record of about 40 winters).

Let E_1 be the vector linking the two weakly-unstable steady states of subsystem (X_1, Y_1, W), and E_2 the corresponding axis for subsystem (X_2, Y_2, W). These two axes correspond to the two leading EOFs of the double Lorenz model. If high-frequency oscillations around the steady states are filtered out from the time series of the model variables, one finds a four-mode PDF for the model state in the plane spanned by E_1

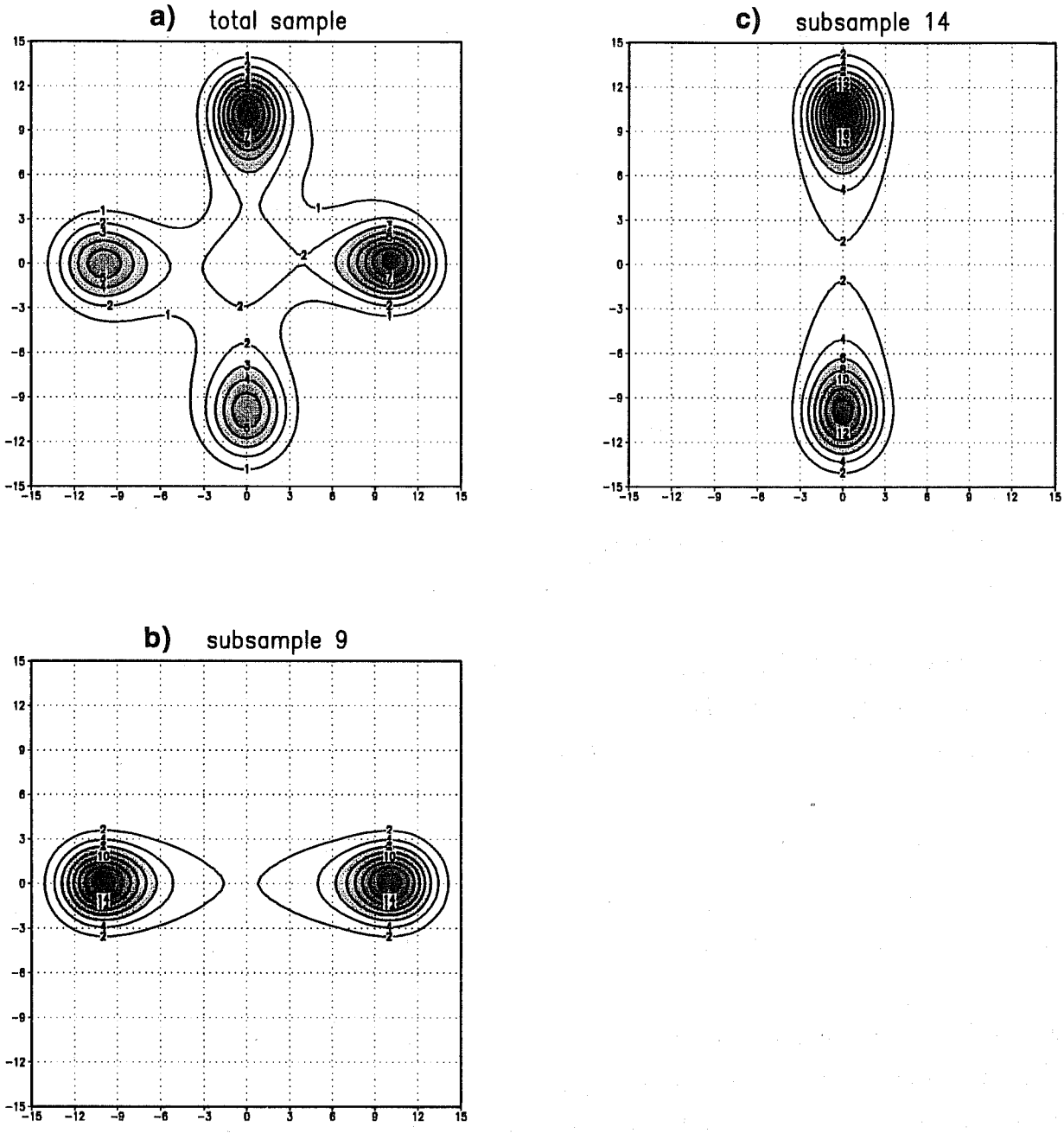

Fig. 5 PDF for the state vector of the 'double Lorenz model' in the plane spanned by the EOFs E_1 and E_2 (x-axis and y-axis respectively); a) for a time interval equivalent to 800 winters; b) and c): for two 40-winter intervals with bimodal PDF.

and E_2 (Fig. 5a). Since two of the regimes are exactly aligned along E_1 and two along E_2, one-dimensional PDFs along the individual EOFs are tri-modal, with the central peak corresponding to the cases in which the system resides in one of the regimes aligned on the other EOF (not shown). Although in the full sample the two subsystems account for the same proportion of variance, as expected from the symmetry between them, it is possible to find 40-winter subsamples in which the variance is almost totally explained by the EOF of one subsystem. In such cases, only two regimes can be detected in the $E_1 - E_2$ plane: the PDF is bimodal along the EOF with larger variance, unimodal along the other axis (see Figs. 5b and 5c, corresponding to two bimodal subsaples).

From a dynamical point of view, this behaviour is originated by the fact that the two subsystems (X_1, Y_1, W) and (X_2, Y_2, W) share the same energy source (i.e. the forcing term for the W variable), and are equally efficient in transferring this energy to the leading variability pattern (note that neither E_1 nor E_2 project on the W variable, and there is no 'external' energy source forcing these patterns directly). In the double Lorenz model this 'chaotic redistribution' of variance is particularly evident because of the complete symmetry between the two subsystem. However, in the real atmosphere or in atmospheric models, a similar behaviour may arise if different low-frequency variability patterns are able to maintain themselves at the expense of the available potential energy of the time-mean flow with comparable efficiency. In such a case, even if two quasi-stationary states exist along one axis in phase space, bimodality along that axis may only be detectable in selected periods, when energy 'happens' to be concentrated along the axis.

b) A perpetual-winter integration of a quasi-geostrophic model.

We shall now discuss an example of fluctuations in the statistical properties of low-frequency variability arising in a fairly realistic model of the atmospheric flow, namely the 3-level quasi-geostrophic (QG) spectral model used in MM93. This model integrates prognostic equations for QG potential vorticity (PV) at the three presure levels of 200, 500 and 800 hPa; the three-dimensional PV and streamfunction fields are linearly related through an appropriate elliptic operator. The equations have the form given by Eq. 1, where the non linear term $\boldsymbol{A}$ represents advection of PV by the rotational flow, and the linear term $\boldsymbol{B}$ includes Ekman dissipation, Newtonian cooling and horizontal diffusion (see MM93 for more details). A time-independent PV forcing (F_d in Eq. 1) is also included in the equations, which in this case represents the (average) combined effects of diabatic heating and advection by the divergent flow. The model has a global domain, and adopts a triangular spectral truncation at total wavenumber 21.

A 'perpetual winter' integration for 108000 days (equivalent to 1200 90-day winters) was carried out, driven by a time-independent forcing determined through the same empirical procedure as in Roads (1987). More

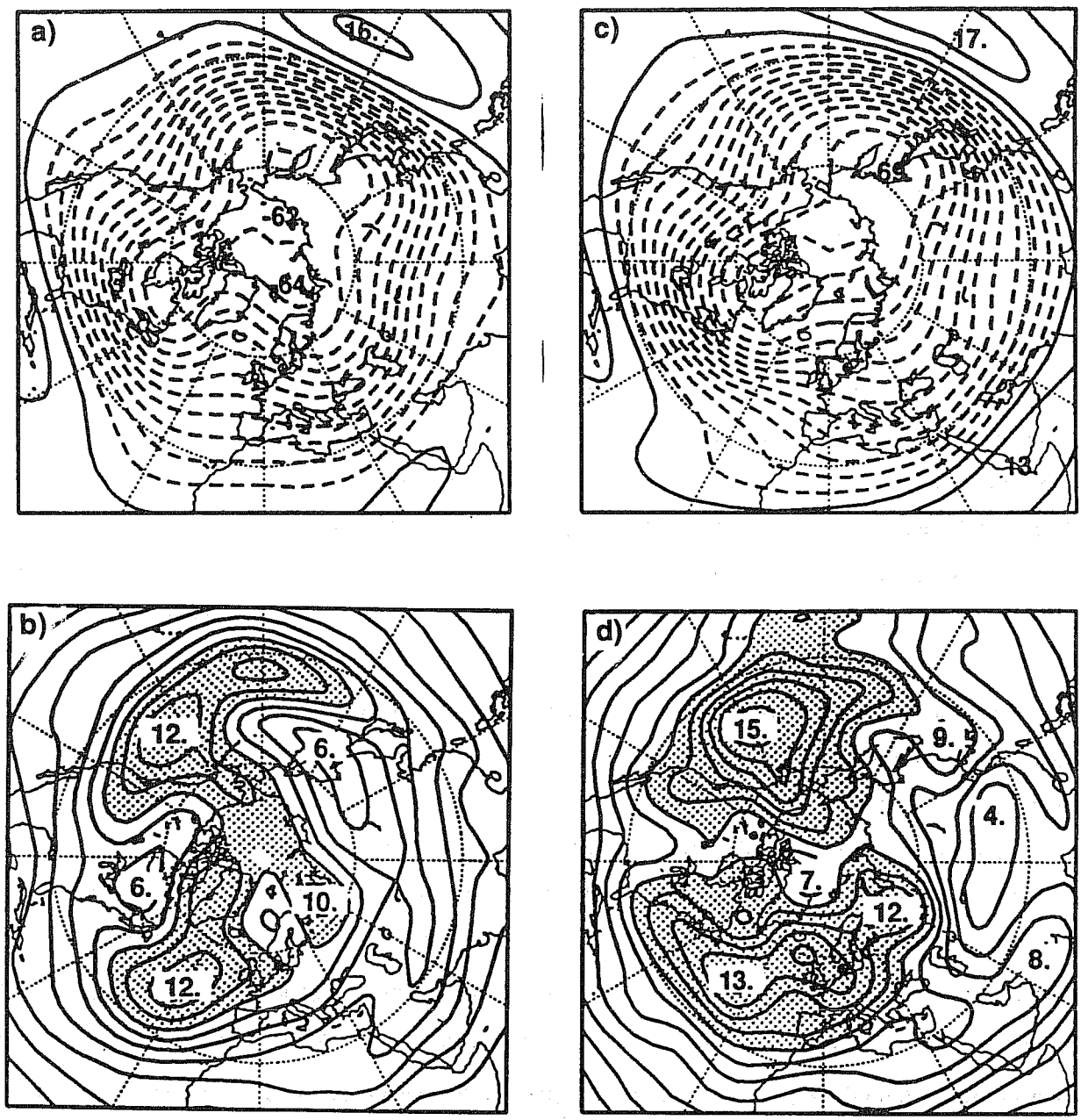

Fig. 6 a) Mean 500 hPa streamfunction from the 1200-winter integration of the QG model with empirical forcing; b) standard deviation of 5-day-means of QG 500 hPa streamfunction; c) and d): as in a) and b), but from ECMWF analyses in January-February 1984-1992.

precisely, the forcing terms were defined as the opposite of the average PV tendencies computed by inserting a large sample of observed streamfunction and PV fields into an unforced version of the model. This is equivalent to assuming that the observed climatology (defined by its mean and variance) represents a statistical equilibrium for the time-averaged equations of the model. The ensemble of observed fields used in the estimate of the forcing were derived from ECMWF analyses of vorticity at the model levels for each day in January and February 1984 to 1992.

Figure 6 shows maps of the mean and standard deviation of the modelled and observed 500 hPa streamfunction. The simulated mean field is quite realistic, with acceptable errors in the amplitude and phase of the stationary waves. The three low-frequency maxima in the North Pacific, North Atlantic and Northwest Siberia are fairly well reproduced, albeit about 10 to 20% lower than observed. (It must be taken into account that the proportion of the variability due to interannual variations of surface forcing, e.g. SST, cannot be simulated in this experiment).

The modelled atmospheric variability was investigated through an EOF analysis of three-dimensional streamfunction, where total energy was chosen as (squared) norm. Fig. 7 shows the pattern of the first five EOFs at the 500 hPa level. EOF 1 is a midlatitude wavenumber-five eddy field superimposed to a strong zonal-mean profile, while EOFs 4 and 5 resemble the North-Atlantic Oscillation (NAO) and Pacific-North-American (PNA) teleconnection patterns respectively (e.g. Wallace and Gutzler 1981; Barnston and Livezey 1987). EOFs 2 and 3 are most likely representative of baroclinic transient waves: in fact, these EOFs disappear if the analysis is performed on 10 day mean fields (not shown). Patterns with a strong zonal component in midlatitude, as EOF 1 here, are not found among the leading EOFs of the observed low-frequency variability, but they do often appear in analyses of long integrations of low-resolution GCMs (e.g Branstator 1990).

Motivated by their similarity to the leading observed teleconnection patterns, we estimated the PDF of model fields (time-filtered with a 10-day running mean) in a bidimensional phase space spanned by EOFs 4 and 5. The PDFs were computed using an iterative bi-dimensional Kernel estimator (Silverman 1986; see also Kimoto and Ghil 1993 and MM93). Fig. 8a shows the PDF estimate relative to the whole dataset (i.e. 1200 winters): the distribution is perfectly unimodal.

A test of stability has been made dividing the sample in two subsamples of 600 winters each, three subsamples of 400 winters each, four subsamples of 300 winters and so on, with the following result: the PDF maintains its unimodal feature only if subsamples including more than 200 winters are considered. For shorter periods there is a 'measurable' (we shall qualify this statement later) probability of obtaining bimodal distributions. When, for example, the complete series of PDFs relative to 12 independent periods

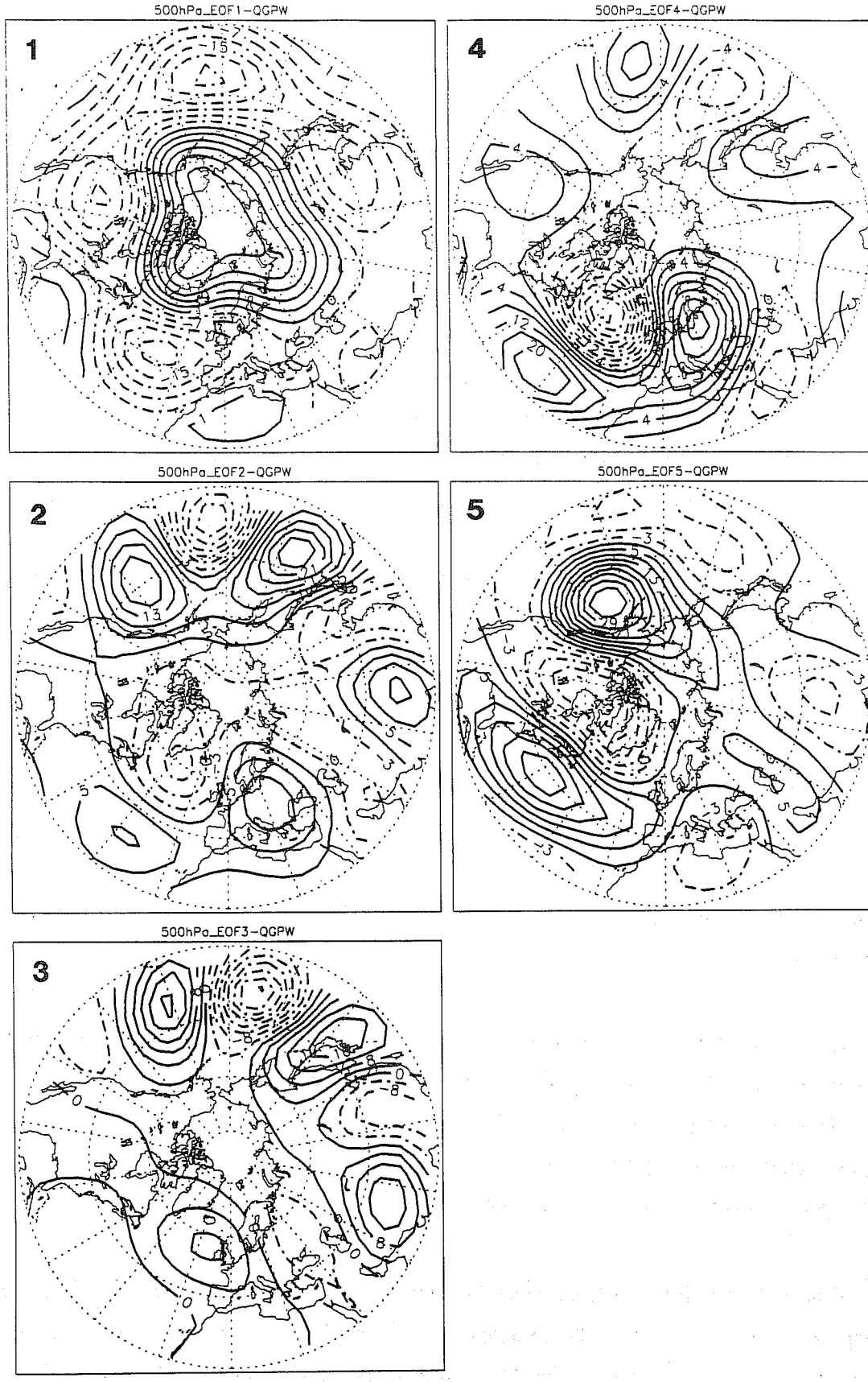

Fig. 7 500-hPa component of the first 5 EOFs of streamfunction from the 1200-winter QG integration.

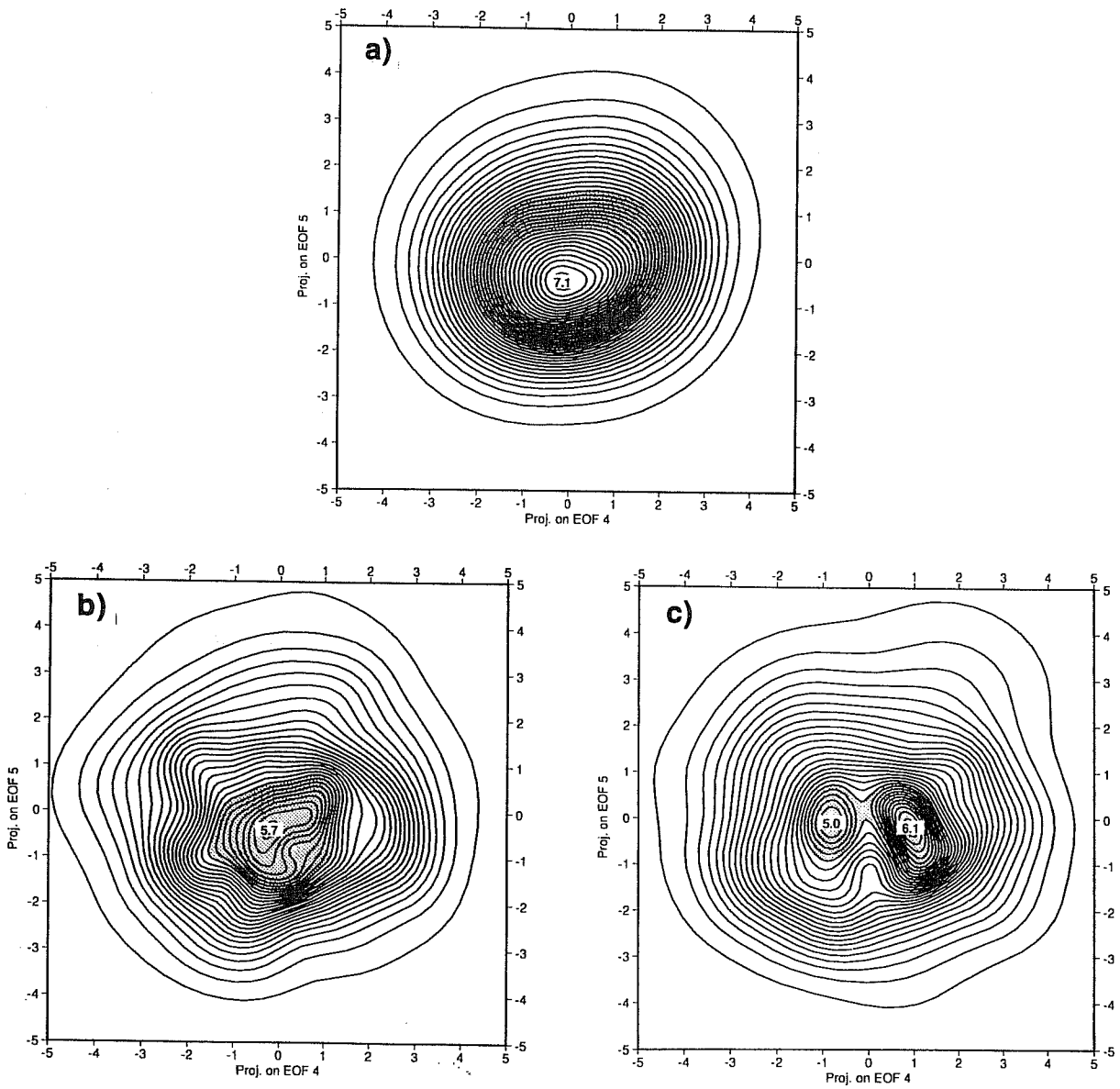

Fig. 8 PDF for the state vector of the QG model in the plane spanned by the EOFs 4 (NAO) and 5 (PNA), from the 1200-winter intgration. a): full 1200-winter sample; b) and c): for two different 40-winter periods.

of 100 winters is considered, 4 distributions with an unquestionable bimodal shape are observed. The probability of finding bimodal distributions is also equal to 33% if one examines a series of 30 successive 40-winter periods (comparable in duration to the time series of available upper-air observations). When bimodality appears, the two maxima are aligned along the axis of EOF 4 (NAO) with a probability two times larger than along the axis of EOF 5 (PNA); bimodality along both axes may occur as well. Examples of two independent 40-winter periods with unimodal and bimodal character along EOF 4 are shown in Fig. 8b-c.

In the absence of further information, one might interpret the variations in the shape of the PDFs as a pure sampling problem, which has no relationship with the dynamics of the system, and is probably due to the use of insufficient smoothing in the estimation of the PDF. To prove that this is not the case, one should demonstrate that multimodality in PDFs from the model integration occurs with a significantly greater frequency than multimodality in samples of similar length originated from a simple red-noise process. Suppose that we had two data series with (a priori known) unimodal gaussian distribution and the same mean, variance, covariance and lag-1 autocorrelation as our EOF coefficients; what would be in this case the probability of obtaining bimodal distributions?

Since the answer to this question depends on the smoothing properties of the PDF estimator, we proceeded as follows. An ensemble of 10 different data samples with bi-dimensional gaussian distributions, having the same statistical properties (i.e. mean, variance, covariance and autocorrelation at lag 1) and the same number of elements as the series of EOF coefficients, were artificially generated using random-number generators. Two-dimensional PDFs from non-overlapping periods of different length were computed, tuning the smoothing parameter as a function of the record length in such a way that the probability of obtaining a bimodal PDF from these red-noise data was always equal to 10%. The same smoothing was then used to estimate the PDFs from model data. The comparison between the frequency of bimodal PDFs in red-noise and model data is summarized in Table 1 below.

Table 1. Frequency of multimodal PDFs in samples of red-noise, multi-normal data and of EOF coefficients from the quasi-geostrophic simulation.

	200 winters	100 winters	40 winters	20 winters
Red-noise	10%	10%	10%	10%
QG model	16%	33%	33%	37%

The frequency of occurrence of bimodality in the QG simulation is about three times larger than the expectation value deduced from the randomly generated distributions (see columns 3 to 5 in Table 1). This suggests that we are not dealing with a trivial sampling problem, but rather with dynamically-induced fluctuactions in the internal variability of the model, on time periods ranging from the interannual to even the inter-centennial scale. Since the only source of potential vorticity in this model is time-independent, one must rule out external causes for the variations of the statistical properties of low-frequency variability. Similarly to the inter-decadal variability in the zonal-mean flow investigated by James and James (1992), differences in intraseasonal variability between successive years, decades and centuries may only arise because of the chaotic nature of the (modelled) atmospheric circulation.

Is it possible to interpret the fluctuations in the QG model statistics using the dynamical concept of energy redistribution illustrated by the 'double Lorenz model' in Sect. 4a? If so, then the periods in which bimodality appears along a given EOF should coincide with periods of above-average variance along the same axis. Besides, to make the comparison more convincing, one should be able to identify a 'complementary' pattern, which shows a reduced variance in the periods when bimodality appears along the former axis.

To address these questions, we shall make use of a statistical technique developed by Ferranti et al. (1994b) to find the spatial patterns that maximize the *difference* in variance between two different datasets (or between two different samples belonging to the same dataset). Ferranti et al. showed that these patterns are the eigenvectors of the difference between the covariance matrices of the first sample (S1 hereafter) and of the second sample (S2 hereafter). Such eigenvectors were called "differential EOFs" (DEOFs). The associated eigenvalues represent the difference between the variances in the two datasets. DEOFs with positive eigenvalues correspond to spatial patterns which have a larger variance in S1 than in S2; conversely, DEOFs with negative eigenvalues correspond to the spatial patterns which have larger variance in S2 than in S1.

In order to carry out this analysis, two appropriate samples of 100 winters each were extracted from the whole dataset of QG-model fields (each winter is a period of 90 consecutive days, but the selected winters may not be consecutive). Sample S1 contains the 100 winters that exhibit the highest amount of variance projected onto the EOF 4 (NAO); this is the EOF along which bimodality was most frequently revealed in the analysis of multi-decadal periods. Conversely, sample S2 consists of those 100 winters which possess the lowest amount of variance projected on the same axis. Since the first 100 EOFs describe 70% of the total variance, projections of S1 and S2 fields onto the subspace generated by these EOFs were used as input data in the DEOF computation.

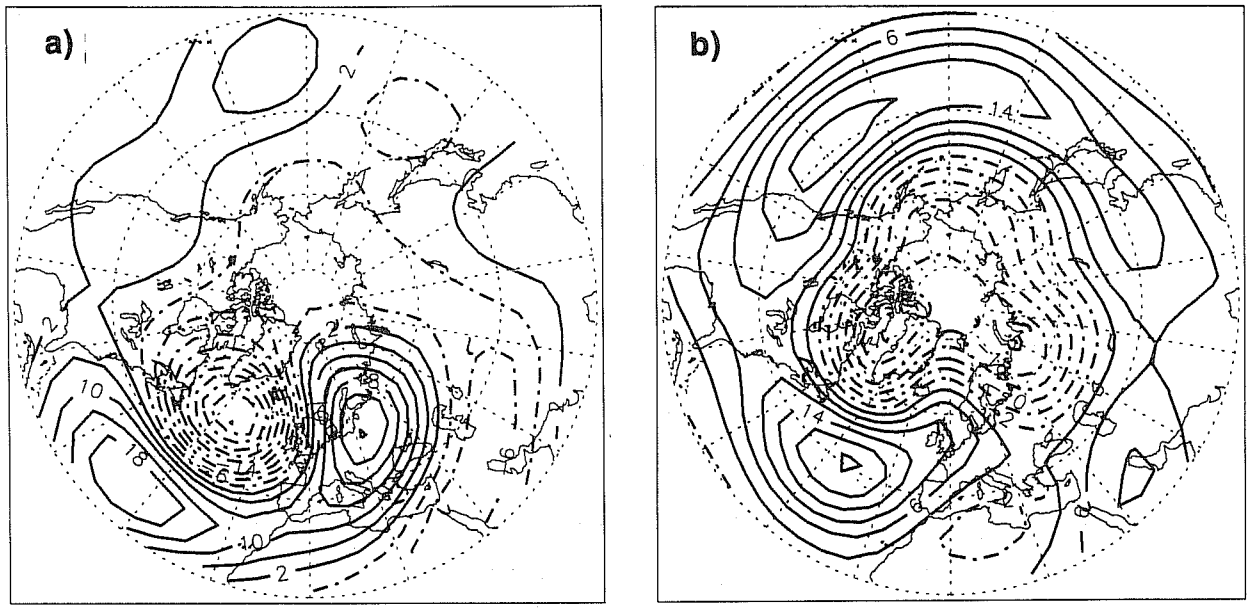

Fig. 9 Differential EOFs +1 (a) and -1 (b) computed from two 100-winter samples S1 and S2, selected according to the variance explained by the QG EOF 4 (NAO).

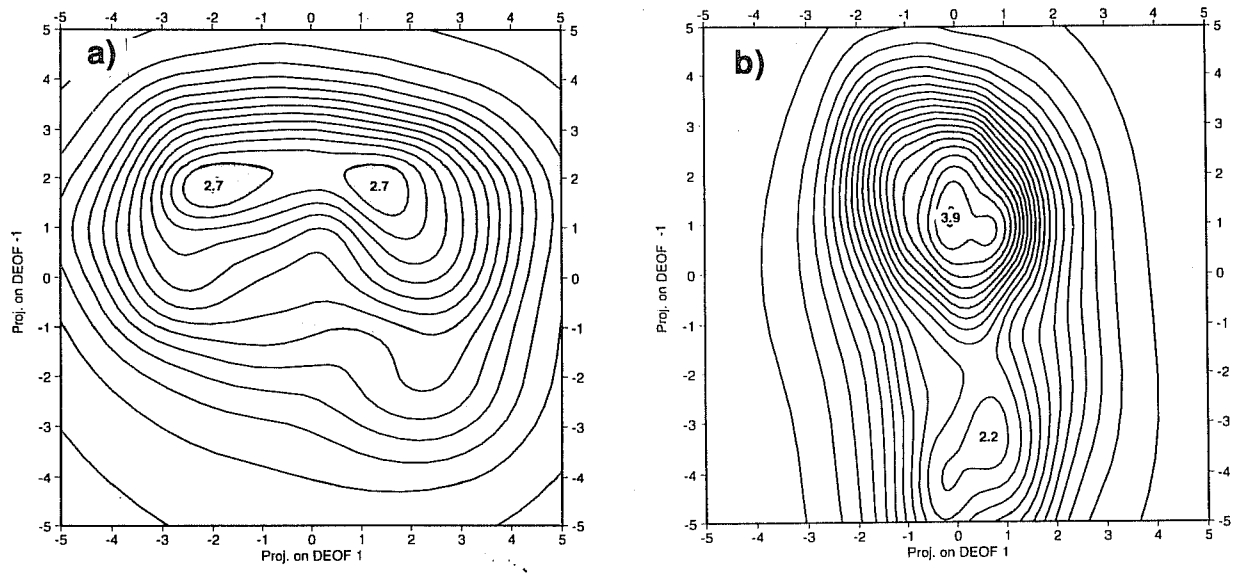

Fig. 10 PDF for the state vector of the QG model in the plane spanned by DEOFs +1 and -1, for the S1 sample (a) and the S2 sample (b).

Figure 9 shows the 500-hPa streamfunction of DEOF +1 and DEOF -1, which represent the spatial patterns associated respectively with the maximum (i.e. largest positive) and to the minimum (i.e largest negative) eigenvalue. The variances of the projections of S1 and S2 fields onto such DEOFs are listed in Table 2.

Table 2. Eigenvalues and variances explained by DEOF +1 and DEOF -1 in samples S1 and S2 (see text for definitions). Values are in m^2s^{-2}.

	Eigenvalue	Variance in S1	Variance in S2
DEOF +1	5.59	8.49	2.90
DEOF -1	-4.84	5.51	10.35

As expected from the definition of S1 and S2, DEOF +1, i.e. the axis which maximizes the variance difference in favour of S1, corresponds to the former EOF 4 (NAO). What could not be expected a priori is that its counterpart with respect to S2, e.g. DEOF -1, is strongly similar to EOF 1, especially in the zonal-mean structure. The variance explained by DEOF -1 doubles when going from S1 to S2; while the variance of DEOF +1 is three times larger in S1 than in S2. Therefore, in periods when a particular pattern, in this case the NAO, becomes more 'active' than usual, it appears to do so at the expense of another preferential pattern of low-frequency variability, and viceversa. Since the EOFs and DEOFs are normalized is such a way that their variance corresponds to the total energy accounted for by each axis, this amounts to an energy redistribution between DEOF +1 and DEOF -1.

PDFs of model states in samples S1 and S2, projected onto the bi-dimensional phase space spanned by DEOF +1 and DEOF -1, are shown in Fig. 10. In both samples, bimodality appears along the axis which explains more variance, as in the case of the 'double Lorenz model' illustrated in Fig. 5. Consequently, the S1 distribution is bimodal along the axis of DEOF +1, while the distribution of S2 is bimodal along DEOF -1.

The results discussed above suggest the following interpretation of the fluctuations affecting low-frequency variability statistics in the QG model atmosphere. As already emphasized, a time- independent empirical forcing represents the only energy source for this system, while dissipative processes are modelled as simple linear sinks of kinetic and available potential energy. In this situation, it can be easily proved that the energy input in a given period depends only on the time-mean state of the system, and it is therefore constant in any period long enough that the mean anomaly vanishes. Conversely, the energy loss due to dissipation depends on both the energy of the time-mean flow and the amount of energy (variance)

accounted for by individual EOFs (because of the EOF orthonormality in an energy metric). It follows that increases in the energy (variance) of one pattern must be compensated by a loss of energy in one or more of the others. These different spatial structures are therefore somehow competitive for the total amount of available energy. If two variability patterns are similarly efficient in extracting energy from the time-mean flow, and their non-linear feedback onto the time-mean flow is also comparable (as in the 'double Lorenz model'), then the chaotic dynamics of the system may produce an alternation of periods with a quite different partition of energy between the two patterns. Regimes associated with quasi-stationary solution along a given axis may become detectable only when the energy accounted for by that axis exceeds a certain threshold.

5. SIMULATION OF INTERANNUAL CHANGES IN LOW-FREQUENCY VARIABILITY.

We shall now turn our attention to the potentially predictable changes in intraseasonal low-frequency variability, namely those induced by interannual variations in boundary forcing. We shall first discuss how the QG model described in the previous section can be modified to include the forcing of the rotational flow by tropical divergence in an explicit way. Then we shall use the model to simulate the differences in low-frequency variability between 1991 and 1992 already described in Sect. 2.

a. Inclusion of an explicit Rossby-wave source in the QG model.

The computation of the PV forcing for the QG model using the 'residual tendency budget' method outlined in Sect. 4b has the disadvantage that the contribution of different dynamical and physical processes to the maintenance of the climatogical flow cannot be separately evaluated. In the model, only orographic forcing is explicitly taken into account by the inclusion of an orographic term in the 800-hPa PV (see MM93). Following Sardeshmukh and Hoskins (1988), we will now add to the prognostic equations of the model a forcing term which represents (in a simplified way) the Rossby-wave source originated by the advection of vorticity by the divergent flow.

Neglecting vertical advection and the twisting term, the vorticity equation in pressure coordinates can be written as:

$$\frac{\partial \zeta}{\partial t} + V_\psi \cdot \nabla (\zeta + f) = - (\zeta + f) D - V_\chi \cdot \nabla (\zeta + f) \qquad (12)$$

where ζ and f are relative and planetary vorticity, D is horizontal divergenge, and the velocity field is

decomposed into its rotational and divergent parts, V_ψ and V_χ. The zonally-asymmetric part of the right-hand-side of Eq. 12, including the stretching term and the advection by the divergent flow, was called the Rossby-wave source by Sardeshmukh and Hoskins (1988). To derive the prognostic eequations of the QG model, Eq. 12 is simplified as follows:

$$\frac{\partial \zeta}{\partial t} + V_\psi \cdot \nabla (\zeta + f) = - f_0 D + S \tag{13}$$

where a constant Coriolis parameter is used in the stretching term, and the remaining terms on the right-hand-side are represented through a time-independent vorticity source S. The stretching term is then expressed through the derivatives of the temperature field to obtain prognostic equations for PV, and the term S is included in the total PV forcing of the model.

Let us now split S into its zonal-mean and eddy components, $[S]$ and S^* respectively. $[S]$, which can be thought of as the net effect of a zonally-symmetric Hadley circulation, contributes to the maintenance of the zonal-mean PV distribution, together with the zonal-mean diabatic heating. An explicit description of all physical processes which maintain the zonal-mean flow is beyond the scope of this work. So, as far as the zonal-mean PV forcing is concerned, we shall still use an empirical approach, and compute this term by requiring that the observed *zonal-mean* climatological flow is a stationary solution of the model equations in the presence of observed, time-averaged PV fluxes by transient eddies with period less than 10 days. We therefore follow a 'perturbation approach' to the determination of the forcing, where we empirically compute the forcing that maintains a given 'basic state' (i.e. the zonal mean climatology with high-frequency transients), while we consider the planetary waves as the non-linear response to a 'perturbative' eddy forcing which is explicitly modelled.

As mentioned above, orography is one source of planetary-wave forcing represented in the model. To such forcing, we add the contribution of the Rossby-wave source S^*, computed from an observed divergence field as follows. Firstly, we simplify S^* by only considering the advection of climatological zonal-mean vorticity by the eddy divergent wind. One reason for such a choice is that it gives a fairly good approximation to the full Rossby-wave source. More fundamentally, we note that such a formulation is independent from the 'response' (i.e. the eddy vorticity field), which may possess more than one equilibrium state; therefore, it may be reasonably thought of as a time-independent forcing, as long as planetary-scale divergence is assumed to be mainly determined by stationary heat sources in the tropics. Given an observed,

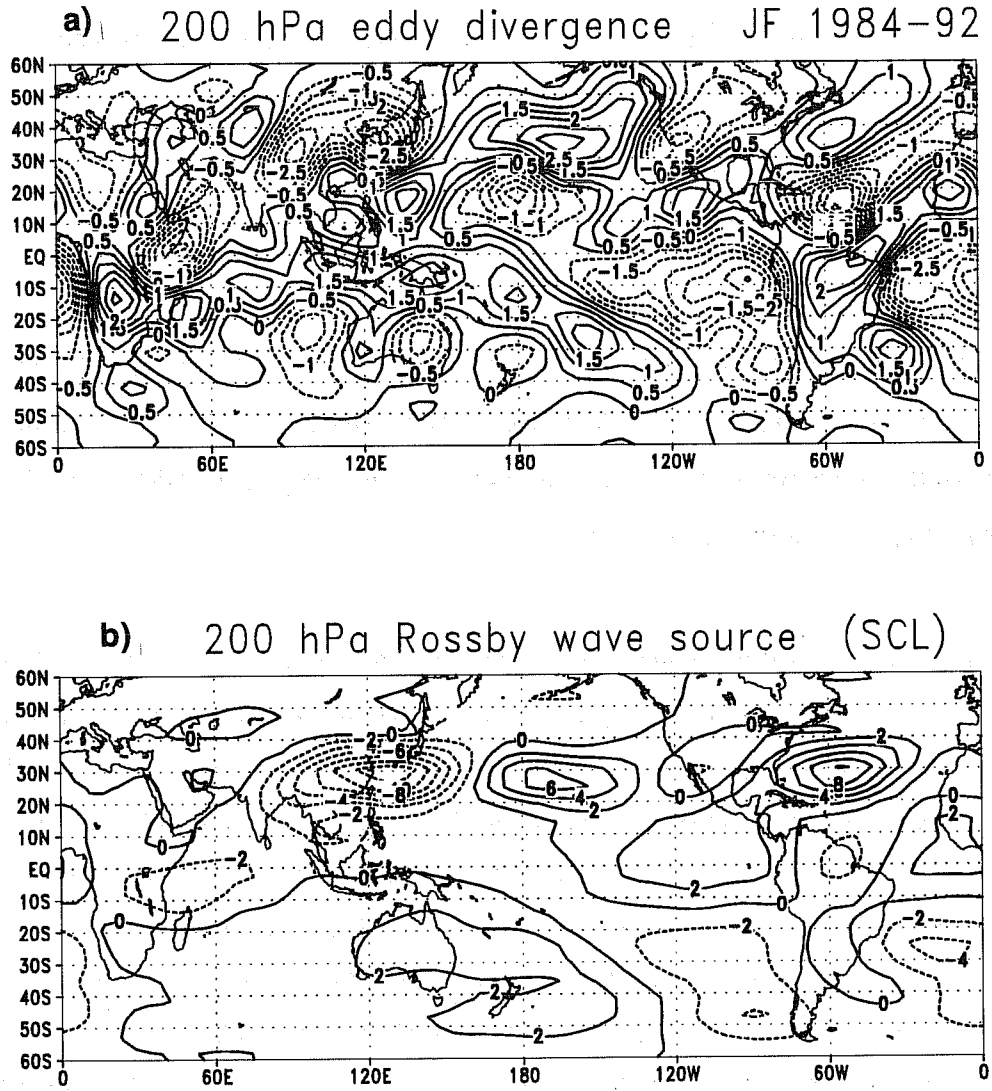

Fig. 11 a) Eddy divergence at 200 hPa, averaged over January-February 1984-94 (from ECMWF analyses); b) Rossby wave source at 200 hPa computed from the field in panel (a).

time-averaged eddy divergence field D^* at one pressure level and the climatological zonal-mean vorticity $[\zeta_c]$, S^* is defined as:

$$S^* = -v_\chi^* \frac{\partial}{a\partial\phi}([\zeta_c]+f) = -\frac{\partial}{a\partial\phi}(\Delta^{-1}D^*)\frac{\partial}{a\partial\phi}([\zeta_c]+f) \tag{14}$$

where a is the Earth's radius, ϕ is latitude, and Δ is the horizontal Laplacian.

Secondly, we assume that the divergence fields at the 200 and 800 hPa levels of the QG model are opposite to each other, while there is no divergence at the 500 hPa level. Divergence at just one level is therefore needed to define S^* in the 3-level QG model; the observed divergence at 200 hPa has been chosen for this purpose. It should be noted that, although the vertical integral of divergence is assumed to be zero, the Rossby-wave source has a non-zero barotropic component because of the different relative vorticity at 200 and 800 hPa.

To test whether the combination of orographic forcing and the simplified Rossby-wave source could account for the observed structure and amplitude of planetary waves, a 7200-day perpetual-winter integration of the QG model has been carried out, using daily ECMWF analyses of vorticity and divergence in January-February 1984 to 1992 to compute climatological fields of $[\zeta]$ and D^*, as well as the contribution of high-frequency transients to the zonal-mean PV balance. Before describing the results of the integration, it is worth looking at the structure of the Rossby wave source. Fig. 11 shows the 9-winter mean of eddy divergence at 200 hPa in the top panel, while the bottom panel shows the pattern of S^* at the same level. The upper-troposphere divergence clearly reflects the distribution of tropical convection areas in the boreal winter, as well as the position of the storm tracks in the northern oceans. Large areas of convergence can be seen over the (relatively cooler) eastern sides of the tropical Pacific and Atlantic. The S^* field is determined by the largest scales of the divergent flow, with the strongest features around 30°N. Two large areas of negative and positive vorticity forcing cover the western and eastern subtropical Pacific respectively, reflecting the strongly asymmetric distribution of convection over this ocean. Another area of large positive forcing is located in the western tropical Atlantic.

For reasons of space, we can only show the results of the perpetual winter integration including both orographic forcing and S^*, and just comment on the relative contributions of the two forcing terms as

estimated from independent integrations. Fig. 12 shows the eddy component of the time-averaged 500-hPa streamfunction over the northern hemisphere, together with the low-frequenct standard deviation computed from 5-day means of the same field. The QG simulation of the wintertime planetary waves is quite realistic in a sector ranging from the central Pacific to the western Atlantic, but it utterly fails to simulate the location and strength of the eastern-Atlantic ridge, and also underestimates the depth of the trough on the eastern Asian border. Consistent with this, the low-frequency variability maximum over the north-eastern Pacific is fairly well reproduced in both amplitude and location, while there is no trace of the maxima close to the British Isles and over western Siberia. The realism of the simulation over the Pacific owes much to the use of the S^* term, which accounts for more than half of the planetary-wave amplitude in this region; conversely, the flow in the Euro-Atlantic sector is only weakly affected by the (modelled) tropical vorticity source.

In the following, we shall therefore restrict our attention to the Pacific-North American sector, where the similarity between observed and modelled flow is strongest. To analyse the modelled low-frequency in further detail, EOFs of 500-hPa 5-day-mean streamfunction in the region (15-75°N, 150°E-60°W) have been computed. The first two EOFs, which account for 26.9% and 16.2% of the total low-frequency variance, are shown in Fig. 13. (These maps show the so-called loading vectors, i.e. the covariance maps between the 500-hPa streamfunction and each standardized principal component.) The first EOF has a clear PNA-like pattern, with two positive centres west of the Hawaii islands and over western North America, and two negative ones in the north-eastern Pacific and in the Florida-Caribbean region. The second EOF has a similar structure to the first one, but shifted 1/4-wavelength upstream, and with the strongest feature centred over the western coast of North America. One may note that the general structure and phase relationship of these two EOF resemble those of the two EOFs from the NCAR-CCM integration shown in Fig. 3a-b (Branstator 1990). It should also be pointed out that the PNA-like pattern appears as the first EOF only when *both* orographic forcing *and* the tropical Rossby-wave source are included in the QG model.

b. Interannual variability between 1991 and 1992.

The different characteristics of the observed crirculation in January-February (JF) 1991 and 1992 have been already discussed in Sect. 2. Here, we briefly remind that, in the Pacific North-American region, the former was a period with large amplitude of planetary waves and above-average low-frequency variability and blocking frequency, while the latter had a prevalence of positive-PNA anomalies and much reduced low-frequency variability in the Pacific (cf. Fig. 2). In the tropical Pacific, an El Niño anomaly was fully developed in early 1992, while in the previous winters SST was higher in the western part of the basin. The difference between the average SST in the two periods (JF 1991 - JF 1992) is shown in Fig. 14a. A large area of positive differences covers the western tropical Pacific, and extends in north-easterly and south-

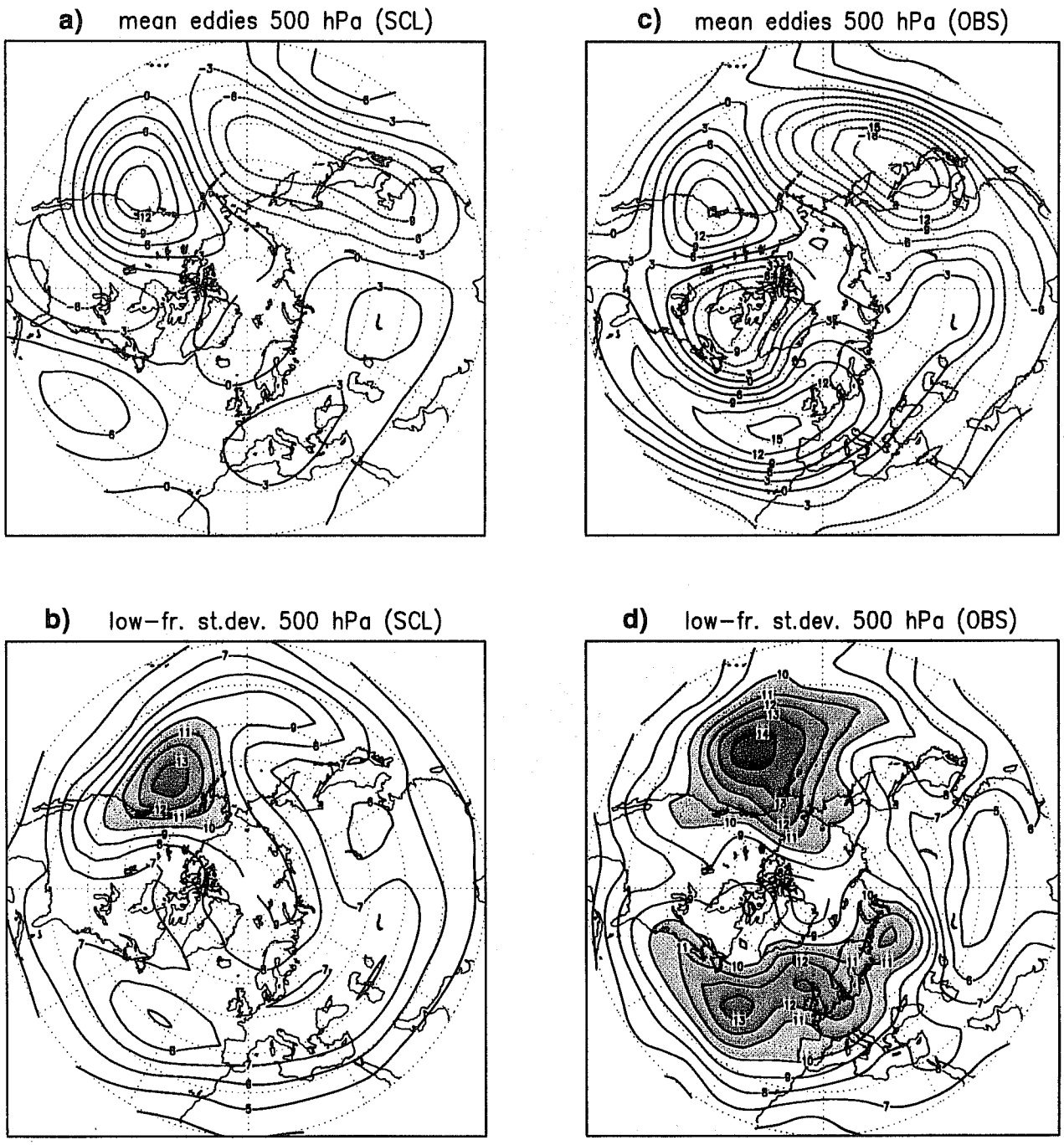

Fig. 12 a) Mean 500 hPa streamfunction eddies from the SCL integration of the QG model, forced by the Rossby wave source shown in Fig. 11b); b) standard deviation of 5-day-mean 500 hPa streamfunction in SCL; c) and d): as in a) and b), but from ECMWF analyses in January-February 1984-1992.

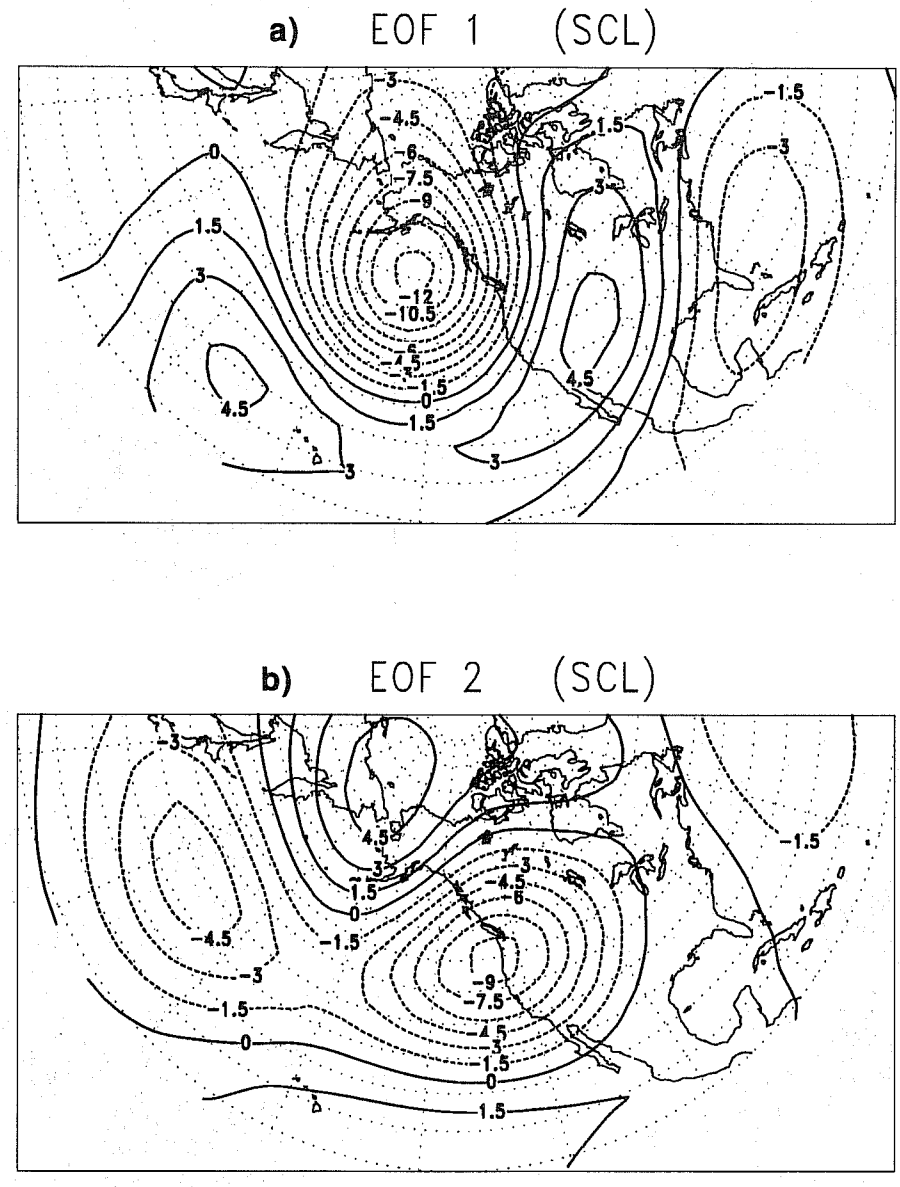

Fig. 13 First two EOFs of 500 hPa streamfunction in the Pacific-North American region, from the SCL integration of the QG model.

easterly direction into the subtropical regions of both hemispheres. Close to the equator, negative differences prevail from the dateline to the western American coast, with a minimum of -2°C around 150°W. This pattern reinforces the climatological thermal contrast between the different parts of the ocean. In Fig. 14b, the difference in 200 hPa divergence, deduced from operational ECMWF analyses, is shown for the same periods. As expected, there is a broad agreement between the sign of the SST and divergence difference patterns, although the equatorial band of negative difference extends further west in the divergence field.

The average 200 hPa divergence fields in JF 1991 and JF 1992 have been used to compute separate estimates of the Rossby-wave source S^*, according to Eq. 14 (not shown for brevity). As the anomalies in SST and vertical motion tend to strengthen or weaken the climatological asymmetry over the Pacific, so the Rossby-wave sources for the two individual winters have a similar pattern to the one computed from a 9-winter average (see Fig. 11b), but with increased and reduced amplitude in 1991 and 1992 respectively. The feature with largest variations ($\pm$30% with respect to the average) is the area of positive vorticity forcing over the eastern Pacific around 25°-30°N, which is also shifted closer to the American coast in JF 1992; the corresponding area of negative forcing in the subtropical western Pacific shows variations in amplitude of $\pm$ 20%, while the Atlantic forcing maximum is quite similar in the two winters.

Two further 7200-day (80-winter) integrations of the QG model have been performed to test the sensitivity of the mean flow and low-frequency variability to the change in tropical forcing, as represented by the S^* term computed from JF 1991 and JF 1992 divergence. As long as one assumes that the changes in tropical divergence are predictable through their dependence on SST anomalies, one can interpret this sensitivity as an estimate of the potential predictability of interannual changes in low-frequency variability statistics. It should be pointed out that the choice of two recent and consecutive years for this experiment was made to minimise the possible impact of changes in the ECMWF model formulation on the interannual variations of analysed divergence. Hereafter, these two integrations will be referred to as to S91 and S92, while the integration with S^* computed from 'climatological' divergence will be indicated as SCL.

Figure 15 shows the difference between the 500 hPa streamfunction of the two experiments, averaged over the 80-winter integration period, and compares this field with its observed counterpart in the Pacific North-American region. The modelled and observed differences are highly correlated: the location and amplitude of the anticyclonic area in the north-eastern Pacific and of the cyclonic areas over western Pacific and Canada are fairly well reproduced, especially if one takes into account the simplicity of the model. The difference is in the sense of increasing the amplitude of the Pacific quasi-stationary waves in S91 with respect to S92. This is better seen in the top panels of Fig. 16, which show the mean streamfunction eddies

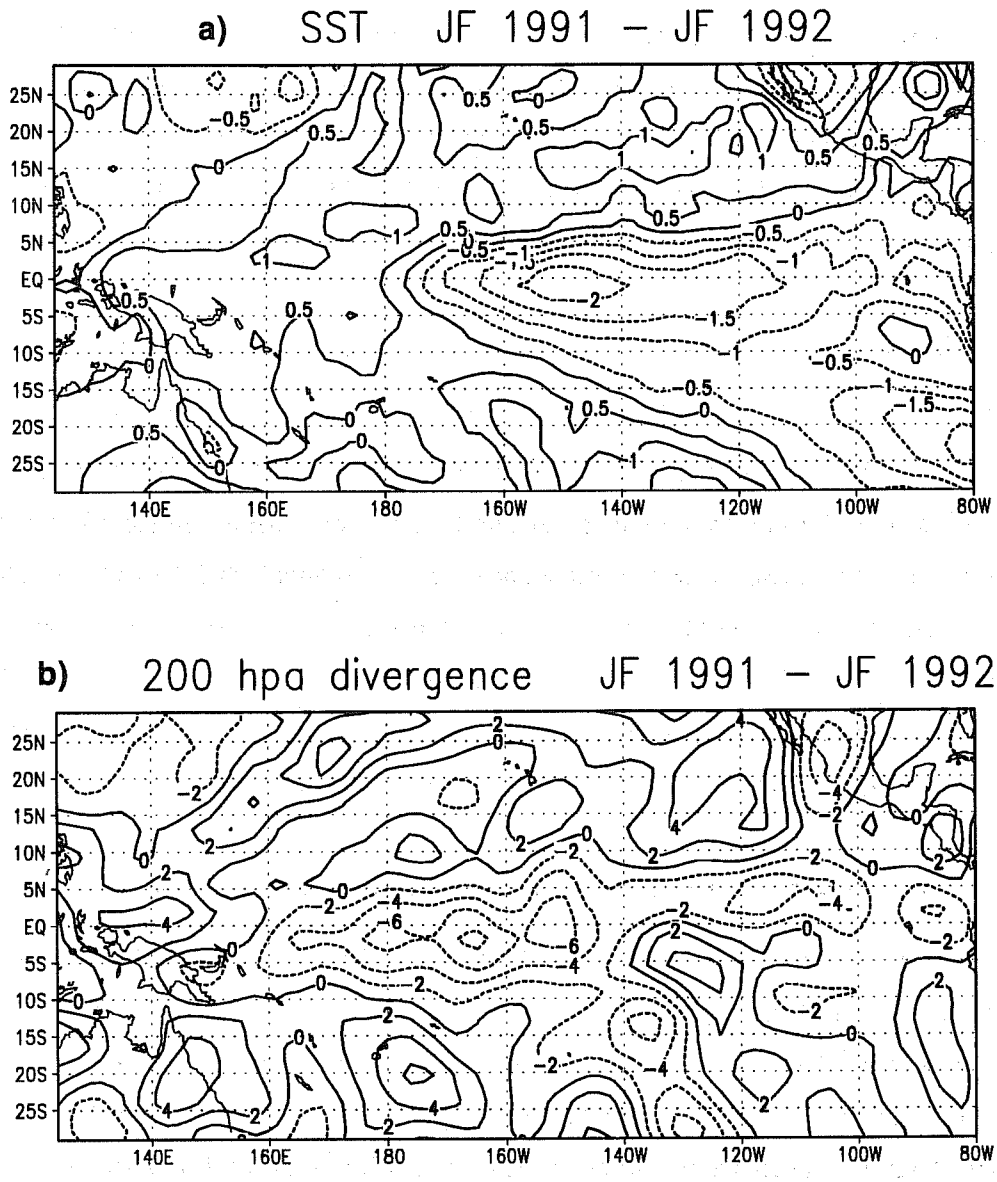

Fig. 14 a) Difference in sea-surface temperature in the tropical Pacific between January-February (JF) 1991 and JF 1992; b) as in a) but for 200 hPa divergence.

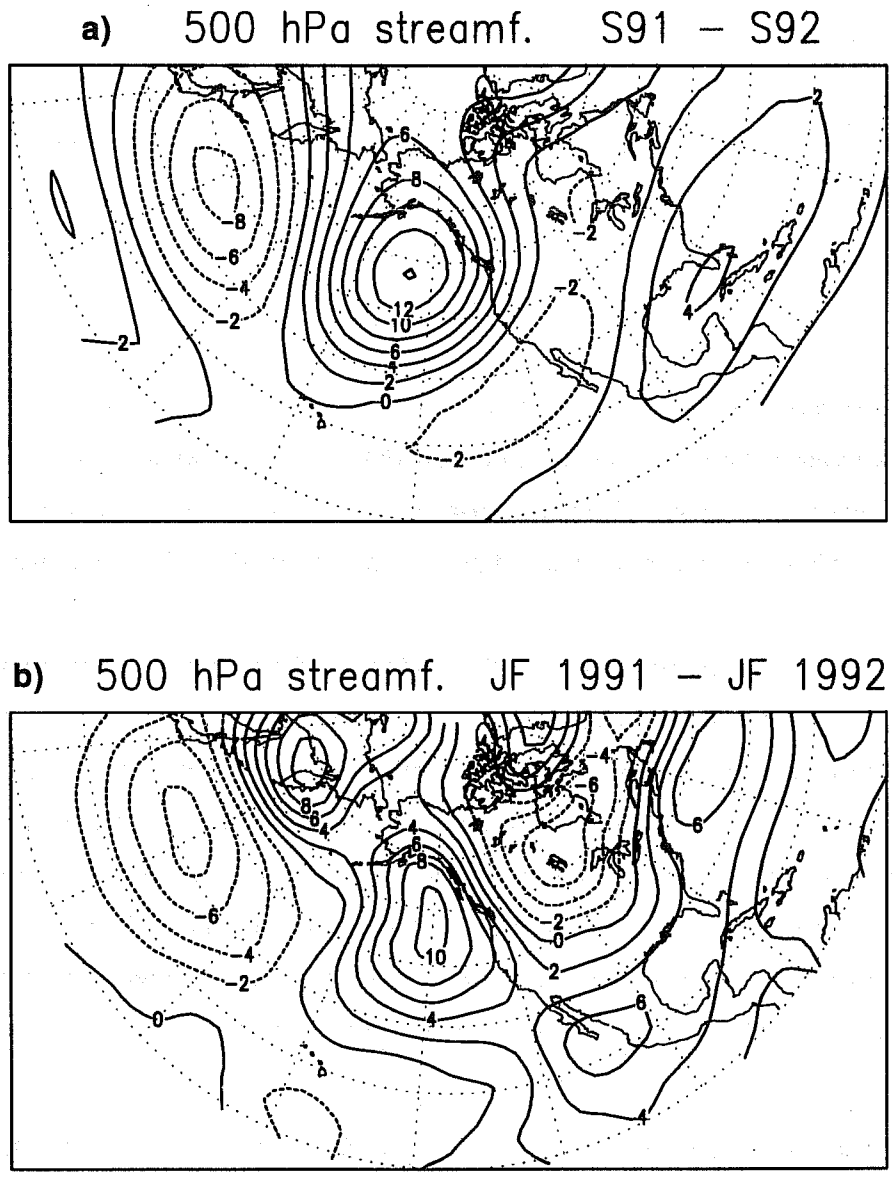

Fig. 15 a) Difference between the mean 500-hPa streamfunction of the S91 and S92 integrations of the QG model, forced by Rossby wave sources computed from observed divergence in JF 1991 and JF 1992 respectively; b) difference in the observed 500-hPa streamfunction in JF 1991 and JF 1992.

from the S91 and S92 integrations separately, on a hemispheric domain. The ridge over the west coast of North America is about 60% stronger in S91 than in S92; in the latter integration, its centre is also shifted westwards as observed (cf. Fig. 2a-c).

The QG model is also successful in reproducing the interannual difference in the amount of Pacific low-frequency variability, shown in Fig. 16b-d as the standard deviation of 5-day mean fields. The maximum value is more than 30% larger in S91 than in S92, and has a more north-westerly position. The modelled variability patterns have a much smoother appearance than the observed ones in Fig. 2b-d, which is not surprising when taking into account that we are comparing 7200-day statistics with 60-day ones! Finally, differences in the structure of the leading EOFs have also been examined. While the first two EOFs of S91 are hardly distinguishable from those of SCL, the first EOF of S92 shows a weaker resemblance to the 'classical' PNA pattern (not shown). However, apart from an eastward shift of its maxima and minima, a better match to the PNA pattern can be obtained by a linear combination of the first two EOFs of S92.

These results suggest that interannual changes in the amplitude and distribution of low-frequency variability may indeed depend on difference in atmospheric forcing, which in turn are caused by anomalies in the lower-boundary conditions (an estimate of statistical significance will be given in the next section). Until now, however, we cannot decide whether the linear or the non-linear theory outlined in Sect. 3 gives a more appropriate dynamical explanation of this phenomenon. To discriminate between the two hypotheses, we have to turn to the analysis of PDFs, introduced in previous sections. In particular, we will look for an indication of separation of flow-regimes in phase space, as an observational support to the non-linear theory of the dependence of multiple quasi-stationary states on forcing parameters.

In the SCL, S91 and S92 integrations discussed above, the differences in the S^* term are not just dependent on one parameter. However, in the tropical Pacific the S^* patterns are fairly well correlated, the main difference being their overall amplitude. Therefore, it is not inappropriate to think of these three integrations as having (approximately) the same forcing pattern, scaled by a parameter which has its minimum value in S92 and its maximum in S91. In the Lorenz model discussed in Sect. 3, an increase of the forcing parameter r leads to a greater distance of the steady states in phase space, and therefore to a greater separation of the two 'modes' of the PDF for the model variables. Can we detect anything similar in the PDF of the state vector of the QG model, when the intensity of the Rossby-wave source is increased?

Figure 17 shows 2-dimensional PDFs for the projections of 500-hPa streamfunction anomalies onto the first two (normalised) EOFs, for the S92 (a), SCL (b) and S91 (c) integrations. Anomalies are defined with respect to the mean state of each run, and the EOFs have also been separately computed from the three

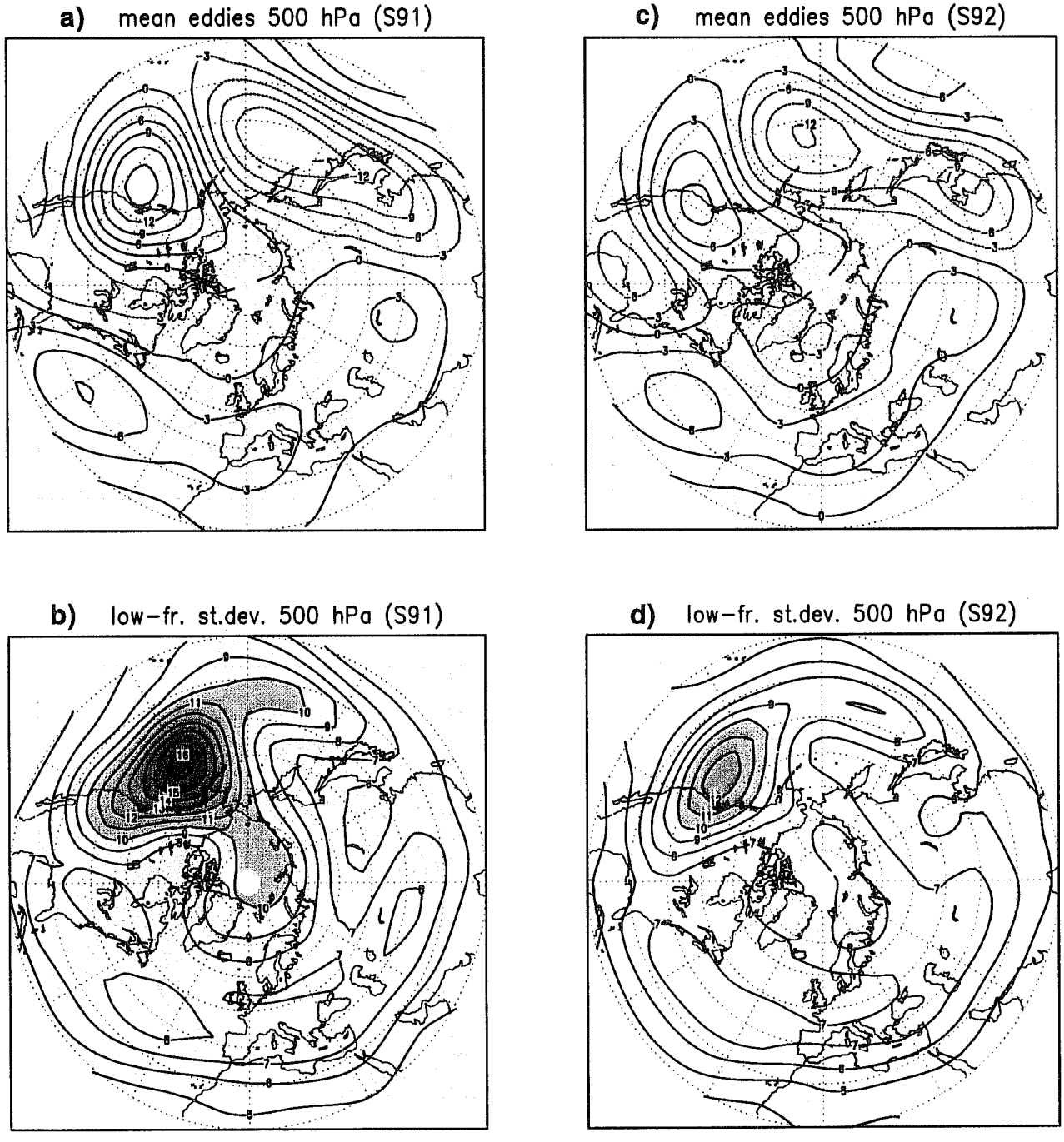

Fig. 16 a) Mean 500-hPa streamfunction eddies from the S91 integration of the QG model; b) standard deviation of 5-day-means in S91; c) and d): as in a) and b), but for the S92 integration.

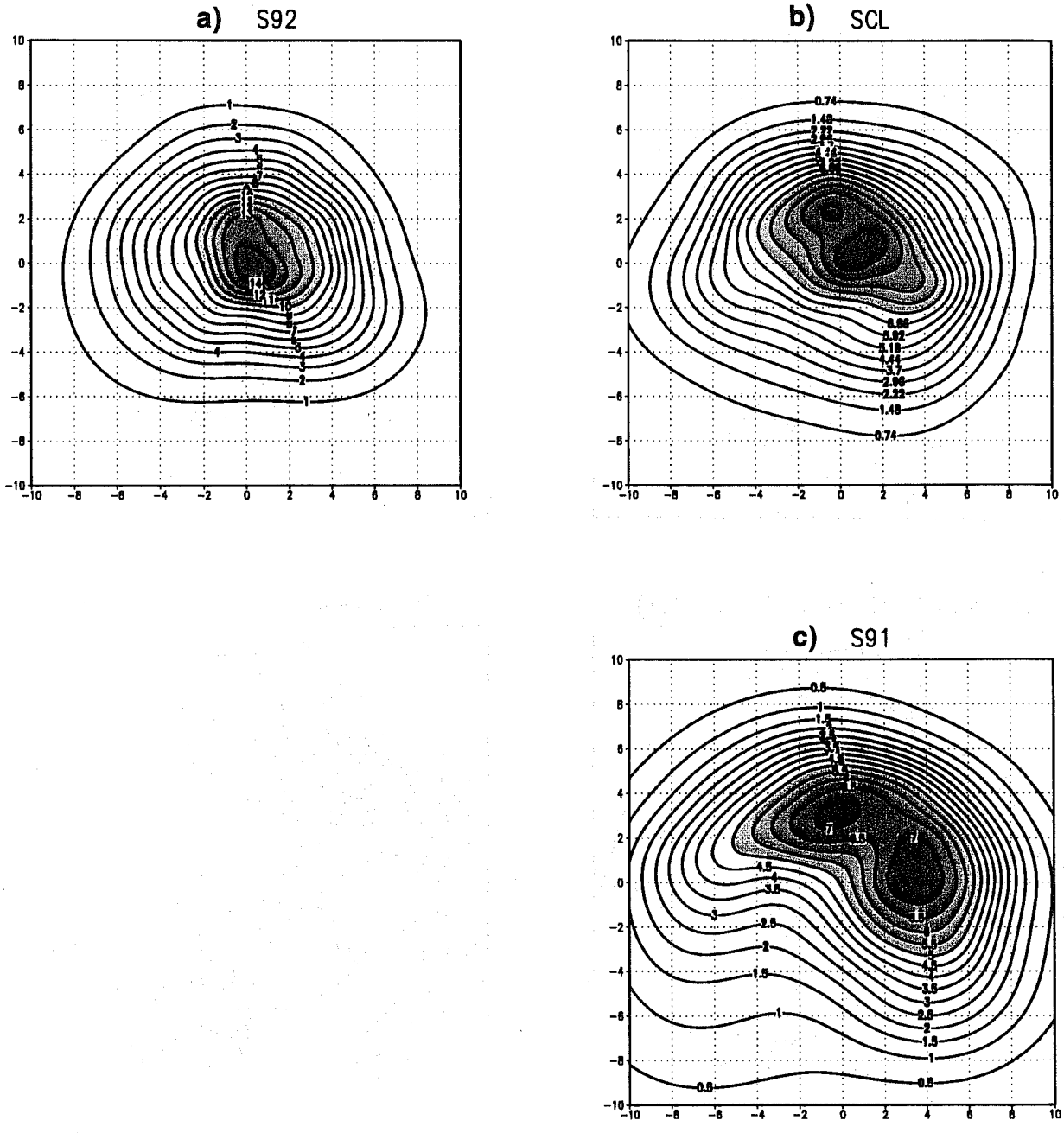

Fig. 17 PDF for the state vector of the QG model in the plane spanned by EOF 1 (x-axis) and EOF 2 (y-axis) of 500-hPa streamfunction in the Pacific-North American region, for the SCL (a), S91 (b) and S92 (c) integrations of the QG model.

experiments (one may prefer to compare projections onto the same EOFs, but the procedure used here has the advantage of treating each integration in exactly the same way.) The PDFs were computed using an iterative bi-dimensional kernel estimator (Silverman 1986), as in Sect. 4.

The integration with the smallest Rossby wave source (S92, panel a) has a unimodal PDF in the space spanned by its two leading EOFs. It either has no distinct flow regimes, or their are too close in phase space to be detected above the 'noise' generated by the different modes of variability of the system. The PDF for SCL (panel b), with 'climatological' S^*, shows instead a weakly bimodal PDF, with the maxima separated by about 2 streamfunction units (1 unit = 10^6 m^2/s, equivalent to about 10 geopotential metres). In the S91 integration (panel c), with the largest tropical forcing among the three, the bimodal nature of the PDF becomes more evident, not so much in the depth of the minimum but rather in the distance between the two maxima, which has now increased to about 5 units. Since the two PDF maxima are located respectively along the first and the second EOF (both with positive sign), and the leading EOFs of S91 and SCL are almost identical, the two regimes of the model are well represented by the two anomaly patterns in Fig. 13.

One can interpret the results above assuming that the increase in tropical forcing from S92 to SCL has brought the modelled circulation in the Pacific-North American sector just beyond a bifurcation point, while the further increase in forcing in S91 has made the model regimes further apart in phase space, leading to a larger amplitude of the low-frequency anomalies. This behaviour is consistent with the response of the ECMWF GCM to an increase in convection over the maritime continent, reported by Ferranti et al. (1994a). From this case study, the non-linear theory of flow regimes appears as a useful tool to study the dependence of statistical properties of low-frequency variability (e.g. its variance distribution and multimodality) on variations in atmospheric forcing.

6. CONCLUSIONS.

In this study, the predictability of the statistical properties of low-frequency variability has been addressed by investigating the dynamical origins of both the 'signal' and the 'noise', which arise respectively from the non-linear response to variations in atmospheric forcing and from chaotic fluctuations in the partition of energy between different variability patterns. Such chaotic fluctuations, which may arise even in relatively simple dynamical systems like the 'double Lorenz model' discussed in Sect. 4a, not only modify the variance explained by individual EOFs of the system, but may either obscure or enhance the 'detectability' of flow regimes in PDFs of model states in periods as long as several decades. On the other

hand, it has been shown that significant variations in both intraseasonal variance and multimodality may arise from interannual modifications of the atmospheric forcing induced by SST anomalies, and communicated to the extratropical flow through the divergent circulation.

After studying the signal and the noise separately, we will address here the crucial question for any predictability problem: is the signal larger than the noise? Further analyses of the integrations discussed in Sect. 5 may provide an answer. We shall again restrict our attention to low-frequency variability in the Pacific-North American sector, as represented by the variance explained by EOF subspaces of various dimensions. As for the real atmosphere over one sector of the Northern Hemisphere, 2 EOFs are sufficient to define the dominant flow regimes, 4 EOFs describe most of the important features of large-scale variability, while 8 EOFs account for almost the whole amount of low-frequency variance.

The histogram in Fig. 18 compares the distribution of 'intraseasonal' variance in the S91 and S92 integrations, defined as the variance in the 8-EOF subspace computed in 80 non-overlapping 90-day periods covering each integration. The mean variance in this subspace is 63 m^2s^{-2} for S91, 39 m^2s^{-2} for S92; in each run the variance in individual 'winters' (i.e. 90-day periods) shows large variations, with about a factor of 3 between the maximum and the minimum value. Still, the two distributions show a relatively small degree of overlapping: a threshold of 50 m^2s^{-2} divides the variance range in two classes, each one populated by about 90% of winters from one integration and 10% from the other.

A more precise estimate of the overlapping between the two distributions is given by the probability that, when one winter is extracted at random from the S91 and another one from the S92 distribution, the variance in the former winter is larger than in the latter (as it is on average). This probability is listed in Table 3a, for subspaces of 1, 2, 4 and 8 EOFs. In addition to the probabilities for individual winters, the table also lists probabilities for averages over 10 randomly-selected winters, which can be interpreted as the result of ensemble averaging over 10 seasonal integrations with the same forcing but different initial conditions. All probabilities were computed from 1000 random selections among the 80 winters of each integration. For any EOF truncation, table 3a shows that the probability of finding a larger variance in one winter from the S91 run is close to 95%; when 10-winter ensembles are considered, each of the 1000 ensembles extracted from S91 had a larger variance than its S92 counterpart. As far as winters 1991 and 1992 are concerned, one can conclude that the signal induced by the difference in tropical forcing is dominant over the noise associated with chaotic fluctuations in variance.

As noted in Sect. 2, these two winters had rather opposite anomalies of the intraseasonal variance in the Pacific. One may wonder whether differences between each of of them and a near-normal situation would still be significantly detectable. Despite the fact that the 9-winter-average divergence used in the SCL

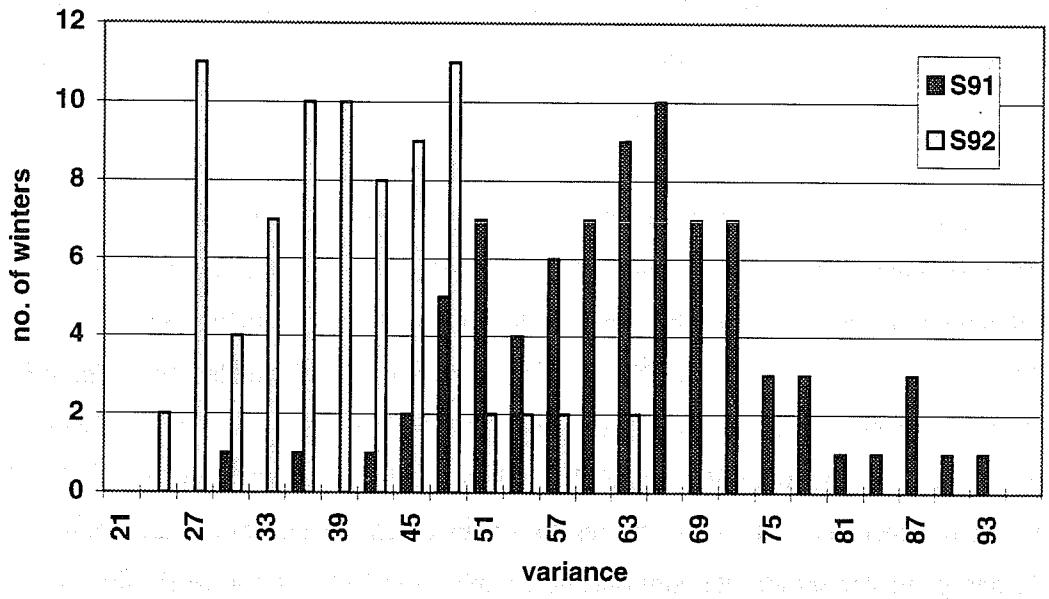

Fig. 18 Distribution of intraseasonal low-frequency variance in the 80 'winters' of the S91 integration (heavy-shaded bars) and the S92 integration (light-shaded bars) of the QG model. Variance is computed from projections onto the first 8 EOFs of 500-hPa streamfunction in the Pacific-North American region.

integration may be affected by changes in the ECMWF data assimilation system, results from the SCL run are indeed intermediate between those of S91 and S92. It is therefore instructive to recompute the probabilities described above, comparing variances from either S91 or S92 with variances from SCL. These probabilities are listed in parts b) and c) of table 3.

The probability of a larger variance in S91 than in SCL is about 85% for individual winters, with small variations between different EOF subspaces; when SCL and S92 are compared, the overlap between the variance distribution is much larger, so that the corresponding probabilities drop to values ranging from 75% (for just the leading EOF) to 65% (for the 8-EOF subspace). Ten-winter ensembles reveal the difference in variance with much larger significance: results for S91 versus SCL are as good as those of S91 vs. S92, while the (smaller) difference between SCL and S92 is still correctly detected in about 95% of the cases. However one should remember that, when the results of an ensemble integration are compared with observations in one particular season, the atmospheric sample only includes one realization, so that the probability of getting the *observed* interannual signal cannot exceed the probability obtained from the distribution of one-winter samples.

Table 3. a): Probability of intraseasonal variance being larger in S91 than in S92 integration, as estimated from individual winters and 10-winter ensembles, and in different EOF subspaces. b): as in a), but for S91 vs. SCL integration. c): as in a), but for SCL vs. S92 integration.

a) S91 vs. S92	1 EOF	2 EOFs	4 EOFs	8 EOFs
1 winter	94.5%	94.5%	95.7%	94.0%
10 winters	100.0%	100.0%	100.0%	100.0%

b) S91 vs. SCL	1 EOF	2 EOFs	4 EOFs	8 EOFs
1 winter	82.7%	82.6%	87.6%	84.5%
10 winters	100.0%	100.0%	100.0%	99.9%

c) SCL vs. S92	1 EOF	2 EOFs	4 EOFs	8 EOFs
1 winter	74.9%	71.7%	71.1%	65.2%
10 winters	99.8%	95.6%	95.2%	94.5%

If the results above suggest that ensemble predictions of intraseasonal variance may have a detectable skill, at least in certain years and geographical areas, they also raise the problem of the effects of systematic errors in the modelled energy sources on the amount and distribution of low-frequency variability in GCMs. Even in state-of-the-art models, differences between the observed and simulated distributions of tropical rainfall may be of the same order of magnitude as interannual differences. Comparing the average wintertime rainfall from ensemble integrations with two cycles of the ECMWF model (which went into operation respectively in June 1990 and March 1994), Brankovic and Molteni (1995) noted a rainfall increase of more than 4 mm/day over large areas of the western tropical Pacific. This is equivalent to an increase of more than 120 $W \cdot m^{-2}$ in the energy flux into the atmospheric column, which in turn (assuming an average albedo of 30%) is comparable to the difference in incoming solar radiation at 20°N between the winter and the summer solstices. Although the effects of other changes in the parametrization schemes could not be discarded, Brankovic and Molteni noted that the improved low-frequency variability and the increase in Pacific blocking frequency in the latest model cycle were consistent with the model sensitivity to western Pacific rainfall found by Ferranti et al. (1994a).

Finally, our results contribute to clarify the debate on the significance of multimodality detected in samples of observed and modelled data. If, as suggested at the end of the previous section, the 'climatological' state of the real atmosphere is just beyond a bifurcation point in phase space, then it is not surprising that detection of multimodality in the atmospheric record or in realistic GCM simulations is so difficult, and so sensitive to sampling. As we have shown here, in multi-dimensional dynamical system such sampling problems are different from those encountered in the analysis of simple red-noise signals. Therefore, successfully testing the statistical significance of bimodality against a red-noise model does not guarantee the reproducibility of such bimodality in a subsequent portion of the observed or modelled record. On the other hand, the fact that bimodality may be undetectable in even some pluri-decadal portions of the record is not a proof that multiple regimes do not exist.

In conclusion, the validity of the theory of flow regimes cannot be assessed only on the base of the 'existence' or 'non-existence' of multimodality. Here, we have used this theory to interpret the relationship between anomalies in atmospheric forcing and fluctuations in the statistical properties of intraseasonal variability. With the increased availability of century-scale integrations of sophisticated GCMs (e.g. Ting and Lau 1993; Von Storch 1994), the analyses performed here on a relatively simple quasi-geostrophic model might be soon repeated on GCMs allowing a much more detailed representation of the atmospheric energy sources, and shed further light on the complex nature of the atmospheric attractor.

ACKNOWLEDGEMENTS.

The authors wish to express their gratitude to S. Tibaldi, whose advice contributed to a better understanding of the results discussed in Sect. 4. Collaboration with scientists in the Diagnostic and Predictability Research Section of ECMWF, particularly with L. Ferranti and T. N. Palmer, also gave a substantial contribution to the development of the ideas expressed in this paper. Thanks are due to S. Jewson for useful discussions as well as practical help with SST data, and to A. Hollingsworth for his comments on the first draft of the paper.

The work of S. Corti was supported by the Commission of the European Communities under contract EV5V-CT93-0279 (Short-term Climate Variability). The GrADS (Grid Analysis and Display System) used to plot most figures in this paper was developed by B. Doty at the Center for Ocean-Land-Atmosphere Studies, Maryland, U.S.A..

REFERENCES.

Andrews, D.G., 1984: On the stability of forced non-zonal flows. *Q.J.R.Meteorol.Soc.*, **110**, 657-662.

Barnston, A.G. and R.E. Livezey, 1987: Classification, seasonality and persistence of low-frequency atmospheric circulation patterns. *Mon.Wea.Rev.*, **115**, 1083-1126.

Brankovic, C. and F. Molteni, 1995: Sensitivity of ECMWF model wintertime climate to model formulation. *ECMWF Technical Memorandum no. 222*, 41 pp.

Brankovic, C., T.N. Palmer and L. Ferranti, 1994: Predictability of seasonal atmospheric variations. *J.Climate*, **7**, 218-237.

Branstator, G., 1985: Analysis of general circulation model sea surface temperature anomaly simulations using a linear model. Part II: Eigenanalysis. *J.Atmos.Sci.*, **42**, 2242-2254.

Branstator, G., 1990: Low-frequency patterns induced by stationary waves. *J.Atmos.Sci.*, **47**, 629-648.

Chen, W.Y. and H. Van den Dool, 1995: Low-frequency anomalies in the NMC MRF model and reality. *J.Climate*, **8**, 1369-1385.

Ferranti, L., F. Molteni, and T.N. Palmer, 1994a: Impact of localized tropical and extra-tropical SST anomalies in ensembles seasonal GCM integrations. *Q.J.R.Meteorol.Soc.*, **120**, 1613-1645.

Ferranti, L., F. Molteni, C. Brankovic and T.N. Palmer, 1994b: Diagnosis of extratropical variability in seasonal integrations of the ECMWF model. *J.Climate*, **7**, 849-868.

Hansen, A.R. and A. Sutera, 1986: On the probability density distribution of large-scale atmospheric wave amplitude. *J.Atmos.Sci.*, **43**, 3250-3265.

Hansen, A.R. and A. Sutera, 1990: Weather regimes in a general circulation model. *J.Atmos.Sci.*, **47**, 380-391.

Hansen, A.R. and A. Sutera, 1995: The probability density distribution of planetary-scale atmospheric wave amplitude revisited. *J.Atmos.Sci.*, **52**, 2463-2472.

Horel, J.D. and J.M. Wallace, 1981: Planetary scale atmospheric phenomena associated with the Southern Oscillation, *Mon.Wea.Rev.*, **109**, 813-829.

Kimoto, M., and M. Ghil, 1993: Multiple flow regimes in the Northern Hemisphere winter. Part I: Methodology and hemispheric regimes. *J.Atmos.Sci.*, **50**, 2625-2643.

Legras, B. and M. Ghil, 1985: Persistent anomalies, blocking and variations in atmospheric predictability. *J.Atmos.Sci.*, **42**, 433-471.

Liu, Q. and J.D. Opsteegh, 1995: Interannual and decadal variations of blocking activity in a quasi-geostrophic model. *Tellus*,

Lorenz, E.N., 1963: Deterministic nonperiodic flow. *J.Atmos.Sci.*, **20**, 130-141.

Marshall, J., and F. Molteni, 1993. Toward a dynamical understanding of planetary-scale flow regimes. *J.Atmos.Sci.*, **50**, 1792-1818.

Miyakoda, K., and J. Sirutis, 1990: Sub-grid scale physics in one-month forecasts. Part II: Systematic error and blocking forecasts. *Mon.Wea.Rev.*, **118**, 1065-1081.

Mo, K.C. and M. Ghil, 1987: Statistics and dynamics of persistent anomalies. *J.Atmos.Sci.*, **44**, 877-901.

Mo, K.C. and M. Ghil, 1988: Cluster analysis of multiple planetary flow regimes. *J.Geophys.Res.*, **93D**, 10927-10952.

Molteni, F., 1996: On the dynamics of planetary flow-regimes. Part I: The role of high-frequency transients. *J.Atmos.Sci.*, in press.

Molteni, F., A. Sutera and N. Tronci, 1988: EOFs of the geopotential eddies at 500 mb in winter and their probability density distributions. *J.Atmos.Sci.*, **45**, 3063-3080.

Molteni, F., S. Tibaldi and T.N. Palmer, 1990: Regimes in the wintertime circulation over northern extratropics. I: Observational evidence. *Q.J.R.Meteorol.Soc.*, **116**, 31-67.

Molteni, F., R. Buizza, T.N. Palmer and T. Petroliagis, 1996: The ECMWF ensemble prediction system: methodology and validation. *Q.J.R.Meteorol.Soc.*, **122**, in press.

Mukougawa, H., 1988: A dynamical model of "quasi-stationary" states in large-scale atmospheric motions. *J.Atmos.Sci.*, **45**, 2868-2888.

Navarra, A., 1993: A new set of orthonormal modes for linearized meteorological problems. *J.Atmos.Sci.*, **50**, 2569-2583.

Navarra, A., and K. Miyakoda, 1988: Anomaly general circulation models. *J.Atmos.Sci.*, **45**, 1509-1530.

Nitsche, G., J.M. Wallace and C. Kooperberg, 1994: Is there evidence of multiple equilibria in planetary wave amplitude statistics? *J.Atmos.Sci.*, **51**, 314-322.

Palmer, T.N., 1988: Medium and extended range predictability and stability of Pacific- North America mode. *Q.J.R.Meteorol.Soc.*, **114**, 691-713.

Palmer, T.N. and D.L.T. Anderson, 1994: The prospects for seasonal forecasting - A review paper. *Q.J.R.Meteorol.Soc.*, **120**, 755-793.

Reinhold, B., and R.T. Pierrehumbert, 1982: Dynamics of weather regimes: quasi-stationary waves and blocking. *Mon.Wea.Rev.*, **110**, 1105-1145.

Roads, J.O., 1987: Predictability in the extended range. *J.Atmos.Sci.*, **44**, 3495-3527.

Sardeshmukh, P.D., and B.J. Hoskins, 1988: On the generation of global rotational flow by steady idealised tropical divergence. *J.Atmos.Sci.*, **45**, 1228-1251.

Silverman, B.W., 1986: *Density Estimation for Statistics and Data Analysis.* Chapman and Hall, New York, 175pp.

Simmons, A.J., J.M. Wallace and G.W. Branstator, 1983: Barotropic wave propagation and instability, and atmospheric teleconnection patterns. *J.Atmos.Sci.*, **40**, 1363-1392.

Simmons, A.J., R. Mureau and T. Petroliagis, 1995: Error growth estimates of predictability from the ECMWF forecasting system. *Q.J.R.Meteorol.Soc.*, **121**, 1739-1771.

Tibaldi, S., and F. Molteni, 1990: On the operational predictability of blocking. *Tellus*, **42A**, 343-365.

Ting, M., and N.-C. Lau, 1993: A diagnostic and modeling study of the monthly mean wintertime anomalies appearing in a 100-year GCM experiment. *J.Atmos.Sci.*, **50**, 2845-2867.

Tracton, M.S. and E. Kalnay, 1993: Operational ensemble prediction at the National Meteorological Center: Practical Aspects. *Wea.Forecasting*, **8**, 379-398.

Tracton, M.S., K. Mo, W. Chen, E. Kalnay, R. Kistler and G. White, 1989: Dynamical extended range forecasting (DERF) at the National Meteorological Center. *Mon.Wea.Rev.*, **117**, 2230-2247.

Vautard, R. and B. Legras, 1988: On the source of midlatitude low-frequency variability. Part II: Nonlinear equilibration of weather regimes. *J.Atmos.Sci.*, **45**, 2845-2867.

Von Storch, J.-S., 1994: Interdecadal variability in a global coupled model. *Tellus*, **46A**, 419-432.

Wallace, J.M. and D.S. Gutzler, 1981: Teleconnections in the geopotential height field during the northern hemisphere winter. *Mon.Wea.Rev.*, **109**, 784-812.